Construction and Building Materials 303 (2021) 124420

Contents lists available at ScienceDirect

Construction and Building Materials

journal homepage: www.elsevier.com/locate/conbuildmat

Advances in the understanding of the role of degree of saturation and water distribution in mechanical behaviour of calcarenites using magnetic resonance imaging technique

Á. Rabat *, R. Tomás, M. Cano

Departamento de Ingeniería Civil, Escuela Politécnica Superior, Universidad de Alicante, P.O. Box 99, E-03080 Alicante, Spain

ARTICLE INFO

Keywords:
Water distribution
Degree of saturation
Mechanical properties
Magnetic Resonance Imaging
Calcarenite

ABSTRACT

A thorough knowledge of the variations of mechanical properties of rock materials with their water content is essential for evaluating the structural behaviour and durability of stone constructions exposed to different moist environments during their lifetime and for solving a broad range of rock mechanics issues. In this study, the effect of degree of saturation (S_r) and water distribution inside pore network on mechanical parameters such as Uniaxial Compressive Strength, Young's modulus, Brazilian Tensile Strength and Point Load Strength Index was assessed for three varieties of a calcarenite. To this aim, the corresponding mechanical tests and Magnetic Resonance Imaging technique were applied during different time intervals in specimens prepared with different S_r values through two different wetting procedures: (1) the oven drying of saturated samples and (2) the water immersion of dry samples. In general terms, the results showed that for small S_r values (≤50%) the specimens wetted using the drying process exhibit greater mechanical properties reductions than those moistened through the immersion process while for higher S_r values (>50%) the decreases are quite similar for both wetting procedures. As a consequence, different negative exponential functions can be used to describe the relationship between water content and mechanical parameters of calcarenites depending on the wetting procedure used. These results can be explained by the different water distributions inside the partial-saturated specimens and the main involved water-weakening mechanisms. Additionally, slightly different correlation functions between the mechanical parameters were established for specimens moistened using each of the wetting processes.

1. Introduction

Sedimentary rocks are frequently used as natural building stones for construction and restoration of open-air structural or ornamental components such as masonry walls, bridge piers, singular or heritage buildings, facades and decorative features. In these situations, rock materials are commonly exposed to wet environments or even in direct contact with water. Therefore, the knowledge of the variations of their mechanical properties with their water content is crucial to assess the safety and durability of these construction elements [1]. Moreover, the effect of water–rock interactions on the mechanical behaviour of rock materials is also relevant for solving a wide range of issues related to rock mechanics applications such as underground works (e.g., tunnelling, mining or drilling), groundwater withdrawal or sub-surface fluid waste disposal [2,3].

Several studies have found significant reductions of the Uniaxial Compressive Strength (UCS) and static Young's modulus (E_{st}) due to water saturation in sedimentary rocks, such as sandstones [4-12], limestones, shales and mudstones [13-16], clay bearing rocks [17] or gypsums [18,19]. These compressive strength reductions and deformability increases varied from 8 to 93% depending on numerous petrological and physical characteristics of rocks. By contrast, the impact of

List of abbreviations and symbols: ρ_{dry}, Dry density; ρ_{sat}, Saturated density; ρ_t, Particle density; ρ_w, Water density; η, Water viscosity; γ, Interfacial tension; θ, Contact angle; BTS, Brazilian Tensile Strength; C, Water absorption coefficient by capillarity; D, Diameter of the specimen; E_{st}, Static Young's modulus; $I_{s(50)}$, Point Load Strength Index; k, Water permeability; L, Length or thickness of the specimen; MRI, Magnetic Resonance Imaging; m_{svac}, Saturated mass of the specimen under vacuum conditions; m_d, Dry mass of the specimen; m_t, Mass of the specimen after immersion or drying during a time t; P, Failure load; PLT, Point Load test; p, Total porosity; p_o, Open porosity; R, Coefficient of correlation; R^2, Coefficient of determination; r_m, Mean pore radius; S_r, Degree of saturation; UCS, Uniaxial Compressive Strength; v_P, P-wave velocity; v_S, S-wave velocity; W_a, Water absorption; w, Water content.

* Corresponding author.
E-mail address: alvaro.rabat@ua.es (Á. Rabat).

https://doi.org/10.1016/j.conbuildmat.2021.124420
Received 27 March 2021; Received in revised form 20 July 2021; Accepted 30 July 2021
Available online 19 August 2021

Table 1
Equations correlating mechanical properties (UCS, E_{st}, BTS and $I_{s(50)}$) and water content (w) of rocks found in previous studies.

Author	Correlation function	R or R^2	Rock type
Correlation between UCS (MPa) and w (%)			
Hawkins and McConnell [50]	$UCS = 39.03 \cdot e^{-1.9601w} + 184.23$	$R = 0.93$	Donegal Quartzite (sandstone)
	$UCS = 29.34 \cdot e^{-0.7646w} + 105.23$	$R = 0.78$	Brownstones (sandstone)
	$UCS = 12.30 \cdot e^{-0.6821w} + 96.27$	$R = 0.71$	Millstone Grit (sandstone)
	$UCS = 36.13 \cdot e^{-0.7794w} + 48.65$	$R = 0.88$	Holcombe Brook Grit (sandstone)
	$UCS = 45.73 \cdot e^{-1.5942w} + 40.29$	$R = 0.97$	Thornhill Rock (sandstone)
	$UCS = 84.01 \cdot e^{-6.4167w} + 230.98$	$R = 0.91$	Crackington Formation (sandstone)
	$UCS = 47.12 \cdot e^{-1.5439w} + 47.65$	$R = 0.95$	Pennant C (sandstone)
	$UCS = 17.27 \cdot e^{-1.0675w} + 67.75$	$R = 0.85$	Penrith C (sandstone)
	$UCS = 6.14 \cdot e^{-0.1104w} + 2.97$	$R = 0.93$	Greensand (sandstone)
Ghafoori et al. [51]	$UCS = 60 \cdot e^{-0.415w}$	$R = 0.93$	Ashfield shale
Lashkaripour and Ajalloeian [15]	$UCS = 88.087 \cdot e^{-0.5443w}$	$R^2 = 0.9617$	Mudshale
	$UCS = 88.781 \cdot e^{-0.445w}$	$R^2 = 0.9892$	Mudstone
	$UCS = 82.279 \cdot e^{-0.4111w}$	$R^2 = 0.9748$	Clayshale
	$UCS = 83.592 \cdot e^{-0.4433w}$	$R^2 = 0.9557$	Mudrocks
Kleb and Vásárhelyi [43]	$UCS = 31.807 \cdot w^{-1.0051}$	$R^2 = 0.661$	Rhyolitic tuff
Romana and Vásárhelyi [52]	$UCS = 92.996 \cdot e^{-0.602w}$	$R^2 = 0.958$	Linton Lane coal mine
	$UCS = 85.65 \cdot e^{-0.358w}$	$R^2 = 0.977$	Rye Hill coal mine
Erguler and Ulusay [17]	$UCS = 31.6 \cdot e^{-0.081w}$	$R = 0.70$	Clay-bearing rocks
Yilmaz [18]	$UCS = 14.68 \cdot e^{-0.8193w} + 24$	$R^2 = 0.93$	Gypsum
AL-Bazali [53]	$UCS = 91.598 \cdot e^{-0.443w}$	$R^2 = 0.994$	Shale A
	$UCS = 86.2 \cdot e^{-0.496w}$	$R^2 = 0.972$	Shale B
	$UCS = 86.895 \cdot e^{-0.419w}$	$R^2 = 0.9762$	Shale C
Yao et al. [46]	$UCS = 23.247 - 2.563 \cdot w$	$R^2 = 0.9758$	Xishahe coal mine
	$UCS = 16.419 - 1.729 \cdot w$	$R^2 = 0.9815$	Huangbaici coal mine
Zhou et al. [49]	$UCS = 19.95 \cdot e^{-0.659w} + 46.80$	$R^2 = 0.944$	Fine-grained sandstone (saturation process)
	$UCS = 19.89 \cdot e^{-0.583w} + 46.21$	$R^2 = 0.901$	Fine-grained sandstone (drying process)
Cherblanc et al. [44]	$UCS = 4.5 \cdot e^{-14.00w} + 6.3$	–	Estaillades limestone
	$UCS = 21.1 \cdot e^{-4.73w} + 43.2$	–	Modern Barutel limestone
	$UCS = 14.6 \cdot e^{-5.23w} + 32.7$	–	Antique Barutel limestone
	$UCS = 11.2 \cdot e^{-1.61w} + 14.9$	–	Yellow Caromb limestone
	$UCS = 10.9 \cdot e^{-1.43w} + 7.25$	–	Grey Caromb limestone
Vergara and Triantafyllidis [47]	$UCS = 28.8 - 0.31 \cdot w^2$	–	Argillaceous swelling rock
Masoumi et al. [45]	$UCS = 43.63 \cdot e^{-0.20w}$	$R^2 = 0.89$	Gosford sandstone
Tang et al. [55]	$UCS = 80.604 \cdot e^{-0.9044w} + 43.17$	$R^2 = 0.9752$	Black sandstone
Tang et al. [56]	$UCS = 55.21 \cdot e^{-0.7502w} + 51.6$	$R^2 = 0.9755$	Red sandstone
Li et al. [33]	$UCS = 57.44 \cdot e^{-0.383w} + 17.71$	$R^2 = 0.965$	Siltstone
Rabat et al. [48]	$UCS = 9.763 \cdot e^{-3.467w} + 19.994$	$R^2 = 0.992$	Calcarenite G-1
	$UCS = 12.830 \cdot e^{-0.733w} + 11.385$	$R^2 = 0.994$	Calcarenite G-2
	$UCS = 16.943 \cdot e^{-3.206w} + 33.294$	$R^2 = 0.939$	Calcarenite G-3
Correlation between E_{st} (GPa) and w (%)			
Erguler and Ulusay [17]	$E_{st} = 3.8 \cdot e^{-0.090w}$	$R = 0.71$	Clay-bearing rocks
Yilmaz [18]	$E_{st} = 13.23 \cdot e^{-0.4701w} + 9.3$	$R^2 = 0.92$	Gypsum
Yao et al. [46]	$E_{st} = 1.766 \cdot e^{-0.149w}$	$R^2 = 0.9862$	Xishahe coal mine
	$E_{st} = 1.659 \cdot e^{-0.154w}$	$R^2 = 0.9426$	Huangbaici coal mine
Zhou et al. [49]	$E_{st} = 1.768 \cdot e^{-0.625w} + 6.25$	$R^2 = 0.882$	Fine-grained sandstone (saturation process)
	$E_{st} = 1.719 \cdot e^{-0.470w} + 6.20$	$R^2 = 0.957$	Fine-grained sandstone (drying process)
Masoumi et al. [45]	$E_{st} = 6.69 \cdot e^{-0.13w}$	$R^2 = 0.86$	Gosford sandstone
Wang et al. [54]	$E_{st} = 10.577 \cdot e^{-0.04w}$	$R^2 = 0.9015$	Sandstone
Tang et al. [55]	$E_{st} = 20.451 - 4.7481 \cdot w$	$R^2 = 0.9953$	Black sandstone
Tang et al. [56]	$E_{st} = 6.183 \cdot e^{-0.6847w} + 10.62$	$R^2 = 0.9769$	Red sandstone
Li et al. [33]	$E_{st} = 6.35 \cdot e^{-0.796w} + 9.79$	$R^2 = 0.936$	Siltstone
Rabat et al. [48]	$E_{st} = 8.150 \cdot e^{-4.688w} + 14.543$	$R^2 = 0.988$	Calcarenite G-1
	$E_{st} = 2.376 \cdot e^{-2.118w} + 8.417$	$R^2 = 0.999$	Calcarenite G-2
	$E_{st} = 13.286 \cdot e^{-6.732w} + 24.990$	$R^2 = 0.947$	Calcarenite G-3
Correlation between BTS (MPa) and w (%)			
Kleb and Vásárhelyi [43]	$BTS = 3.1152 \cdot w^{-1.0211}$	$R^2 = 0.6635$	Rhyolitic tuff
Erguler and Ulusay [17]	$BTS = 3.4 \cdot e^{-0.1014w}$	$R = 0.73$	Clay-bearing rocks

(*continued on next page*)

Table 1 (*continued*)

Author	Correlation function	R or R^2	Rock type
Cherblanc et al. [44]	$BTS = 0.85 \cdot e^{-11.90w} + 2.14$	–	Estaillades limestone
	$BTS = 4.69 \cdot e^{-10.10w} + 6.22$	–	Modern Barutel limestone
	$BTS = 3.47 \cdot e^{-5.64w} + 4.70$	–	Antique Barutel limestone
	$BTS = 2.06 \cdot e^{-2.40w} + 3.66$	–	Yellow Caromb limestone
	$BTS = 2.27 \cdot e^{-2.37w} + 1.31$	–	Grey Caromb limestone
Masoumi et al. [45]	$BTS = 4.12 \cdot e^{-0.15w}$	$R^2 = 0.80$	Gosford sandstone
Rabat et al. [48]	$BTS = 1.139 \cdot e^{-2.857w} + 3.327$	$R^2 = 0.895$	Calcarenite G-1
	$BTS = 2.989 \cdot e^{-0.735w} + 0.995$	$R^2 = 0.966$	Calcarenite G-2
	$BTS = 3.174 \cdot e^{-1.267w} + 4.102$	$R^2 = 0.997$	Calcarenite G-3
Correlation between $I_{S(50)}$ (MPa) and w (%)			
Masoumi et al. [45]	$I_{S(50)} = 3.69 \cdot e^{-0.17w}$	$R^2 = 0.99$	Gosford sandstone
Rabat et al. [48]	$I_{S(50)} = 0.988 \cdot e^{-5.534w} + 1.980$	$R^2 = 0.996$	Calcarenite G-1
	$I_{S(50)} = 0.908 \cdot e^{-1.556w} + 1.111$	$R^2 = 0.988$	Calcarenite G-2
	$I_{S(50)} = 10.640 \cdot e^{-15.617w} + 3.880$	$R^2 = 0.893$	Calcarenite G-3

water on tensile strength properties such as Brazilian Tensile Strength (BTS) and Point Load Strength Index ($I_{s(50)}$) or shear strength parameters has been scarcely studied. Concerning BTS, Ojo and Brook [20] and Karakul and Ulusay [21] reported reductions of 50 and 63% in British and Turkish sandstones, respectively. Also Wong and Jong [22] obtained decreases of 49–52% in gypsums, while Gholami and Rasouli [23] found losses of 21% in an Iranian slate. With respect to $I_{s(50)}$, Broch [24] obtained reductions of 15% in several sedimentary and metamorphic rocks, Kohno and Maeda [25] found decreases of 59% in volcaniclastic materials and Kahraman [26] reported losses of 35% in pyroclastic rocks. Regarding shear strength parameters, Li et al. [27] and Rabat et al. [28] obtained important cohesion reductions (of 9% in sandstones and of 35–53% in limestones) and also significant friction angles decreases (of 14% and of 5–22%, for sandstones and limestones, respectively). All the above mentioned strength and stiffness drops induced by water and the non-durable behaviour exhibited by some rock types (mainly mudstones and shales), which disintegrate when subjected to variations in moisture content, can trigger geotechnical issues (such as slope or pillar instabilities, embankments failures, ground subsidence or landslides) [29] or safety and deterioration problems in stone buildings [30].

Numerous mechanisms have been suggested to explain the underlying causes of this water-weakening effect: a) chemical causes such as the dissolution of calcite [31,32] and the swelling of clay minerals [17,33]; b) the hydrolysis of strongly bonded and highly stressed Si-O-Si groups in quartz, that reduces the stress threshold of crack growth at crack tips due to the replacement of -Si-O- groups by weaker -Si-OH-groups, which can accelerate the cracking velocity of microcracks (stress corrosion) [34-36]; c) the reduction of surface energy of the grains due to physical adsorption from the nearby water (Rehbinder effect) [37]; d) the suction decrease caused by an increment of the degree of water saturation, which weakens the capillary attraction or the bounding effect related with the existence of a meniscus in unsaturated circumstances [38,39]; e) others, such as pore pressure increase or coefficient of friction reduction [40]. Furthermore, Baud et al. [41] used experimental data and micromechanical models to satisfactorily explain that the reduction of surface free energy and friction coefficient were the main causes of water weakening effect in porous sandstones. In any case, whatever the reasons of this water-weakening effect, the quantity of water contained inside the rocks always plays an important role in the decreases of its mechanical properties [42]. Therefore, it is practical to obtain empirical relationships between the degree of saturation (or moisture content) and the mechanical parameters of rocks.

The majority of the abovementioned studies have compared strength and deformability properties of rocks in dry and fully saturated conditions, ignoring the effect of partial water saturation on their mechanical behaviour. Nevertheless, some authors have also proposed negative exponential, power o linear functions to describe the relationship between water content (w) and UCS [15,17,18,33,43-55]. The variations of E_{st}, BTS and $I_{s(50)}$ with water content have been less studied, although similar correlation function types have been found (Table 1).

Another aspect to note is that these researchers have frequently used inconsistent laboratory techniques for obtaining fully, partially water saturated or dry samples and for determining their water absorption or degree of saturation (S_r). As a consequence, the results presented in previous studies are usually difficult to compare [57]. In this connection, two procedures have been principally described in literature for the partial water saturation of rock specimens: (1) the oven drying of saturated samples or (2) the water immersion of dry samples, both during different time intervals. Also, this variety of procedures used in previous works to obtain partial water saturation specimens suggests that the effect of water distribution inside rocks on their mechanical behaviour have been neglected. As regard the latter, for two rock samples with the same moisture, one of them could have wet its outer zone but dry its inner zone while, on the contrary, the other could have dry its outer zone and wet its inner zone. This evidences that the procedure used to obtain partial-saturated specimens could play a key role in the relationship between water content and mechanical parameters. In this sense, very few studies have been conducted on this topic. One of them was performed by Zhou et al. [49], who used the Nuclear Magnetic Resonance (NMR) technique to study the water distribution in a Chinese fine-grained sandstone prepared with different water contents and its impact on static and dynamic mechanical properties. They concluded that water distribution inside this rock had a significant influence on BTS and a less influence on UCS and E_{st}. A recent paper written by Fu et al. [58] analysed the imbibition of capillary water into the sandstones using NMR and numerical DEM modeling. Also, they performed UCS tests on specimens that had been immersed in water during different periods of time. Their findings displayed that, when the water is confined to the outer edge of the specimen, it was still strong due to the dry core of the sample. As water penetrated into the core of the specimen, higher UCS reductions were observed. In addition, other recent study was carried out by Liu et al. [59], who quantified the evolution of water distribution inside a sandstone with soaking time using a red ink dissolution and a high-resolution camera. They indicated that water distribution significantly affects the UCS and E_{st} values and the failure mode of sandstone specimens. These inconsistent findings suggest that deeper and further research on this subject is needed, which has motivated the present publication.

In this work, three varieties of a calcarenite stone widely present in south-eastern part of Spain and that belong to a transgressive unit of Middle-Late Miocene era were used. These rock materials are extensively used in civil engineering projects and architectural constructions which are usually exposed to moisture changes during their lifetime due

to the water uptake by capillary uprise from the ground, rainfall, spout water or wind-driven water [60]. Therefore, a comprehensive knowledge of the variation of their mechanical parameters with their degree of water saturation is an important pending issue to be explored. In this sense, previous works performed on these rock materials have shown that UCS and E_{st} values suffer important reductions when they became fully saturated [11] or when they are exposed to high environmental relative humidities [48]. However, the role of water distribution inside their pore network on the water-weakening effect has not been studied to date. The present paper tries to fill this gap.

Specifically, the main objectives of this study are: (1) to determine the influence of water content (or degree of saturation) on the UCS, E_{st}, BTS, $I_{s(50)}$ and the failure mode of three varieties of a porous calcarenite stone for different procedures of saturation of the samples (i.e., immersion and drying processes); (2) to obtain and compare the water distribution inside wet rock specimens prepared with the two different water-saturation procedures by using the MRI technique; (3) to assess the effect of the water distribution (or the partial water saturation procedure used) on their mechanical parameters; (4) to establish correlation functions between the abovementioned mechanical properties.

2. Materials and methods

2.1. Sample preparation and determination of physical and microscopic properties

Three fine- and medium-grained calcarenite varieties (labelled as S-1, S-2 and S-3) extracted from a quarry located in the municipality of Elda (Alicante, SE Spain) were used in this study. To perform the experimental research, cylindrical core samples of 28 and 52 mm in diameter were drilled in the direction perpendicular to the sedimentary bedding from intact and homogeneous rock blocks using a diamond drill rig. Then, the samples were cut using an electrical saw in order to obtain specimens with the required length to carry out the corresponding mechanical tests according to the ISRM Suggested Methods [61].

Petrological characterization of the three rock varieties was carried out using petrographic and scanning electron microscopic (SEM) examinations as well as X-ray diffraction (XRD) and fluorescence (XRF) techniques. Physical characterization was performed using conventional procedures. In particular, dry (ρ_{dry}) and saturated (ρ_{sat}) densities, open (p_o) and total (p) porosities and water absorption (W_a) were obtained following the UNE-EN 1936 standard [62]. Particle density (ρ_t) was determined through pycnometers method following the UNE 103–302-94 standard [63]. Moreover, the pore throat size distribution of calcarenites were obtained through the Mercury Intrusion Porosimetry (MIP) technique using a porosimeter equipped with two low- and two high-pressure stations. Additionally, MIP tests allowed to obtain other properties of pore network such as tortuosity and intra- and inter-particle porosities, which were calculated using PoroWin version 8.1 software (PoreMaster, Quantachrome Instruments) [64]. Water absorption coefficient by capillarity (C) was obtained in accordance with UNE-EN 1925:1999 standard by Bateig [65]. Then, permeability (k) was estimated indirectly in tested rocks from their capillary imbibition and pore structure using Eq. (1) proposed by Benavente et al. [66].

$$k = C^2 \cdot \frac{\eta \cdot r_m}{4 \cdot p_o \cdot \rho_w^2 \cdot \gamma \cdot \cos\theta} \quad (1)$$

which considers the water absorption coefficient by capillarity (C), water parameters (density, ρ_w, and viscosity, η), wetting (interfacial tension, γ, and contact angle, θ) and pore structure of rocks (mean pore radius, r_m, and porosity, p_o).

P- and S-wave velocities (v_P and v_S, respectively) of dry specimens were measured along the sample axis (i.e. perpendicular to bedding) and were computed from the ratio of the sample length to the transit time of the pulse by using a signal emitting-receiving device and following the UNE-EN 14579 standard [67].

2.2. Procedures for obtaining partially water saturated specimens

2.2.1. Procedure 1: Water saturation by immersion under atmospheric pressure during different time intervals

Five cylindrical specimens of each calcarenite variety of 28 mm in diameter and 70–75 mm in length were used to obtain the variation of the S_r with the time of water immersion under atmospheric pressure. Specifically, the following process was performed. Firstly, the specimens were dried at 70 °C inside a ventilated oven until a constant mass was reached (the difference between two weighings carried out in a 24-hour interval was not>0.1% of the mass of the sample). After that, the specimens were kept in a desiccator until they reached the room temperature (20 ± 5 °C) and later their dry mass (m_d) was measured with an accuracy of 0.01 g. Subsequently, the dry samples were completely submerged in a vessel with water at ambient laboratory temperature and at atmospheric pressure and the timer was started. At certain time intervals, initially very short and then longer, the specimens were removed from the vessel, dried slightly with a damp cloth to remove the water droplets of their surface, weighed immediately (m_t) and then reintroduced into the vessel with water. The time intervals between each weighing were 1 min in the range from 0 to 15 min, 5 min in the range from 15 to 60 min, 10 min in the range from 1 to 2 h, 20 min in the range from 2 to 4 h, and 1 h from 4 h up to obtaining a constant mass of the sample (i.e, the saturated mass at atmospheric pressure). Finally, the specimens were forcibly-saturated by means of a vacuum chamber until they reached a constant mass, obtaining the saturated mass under vacuum conditions (m_{Svac}). The S_r for each water-immersion time interval was calculated using Eq. (2):

$$S_r(\%) = \frac{m_t - m_d}{m_{Svac} - m_d} \cdot 100 \quad (2)$$

After defining the relationship between the immersion time and the S_r value achieved for each calcarenite variety, the time required to obtain S_r values of 25, 50 and 75% was calculated by interpolation. Then, these estimations were utilized to prepare specimens with these water contents in order to perform the mechanical tests.

2.2.2. Procedure 2: Oven drying of saturated samples during different time intervals

The variation of the S_r with the drying time was determined using five cylindrical specimens of 28 mm in diameter and 70–75 mm in length of each calcarenite variety. The following steps were taken: Firstly, the samples were dried at 70 °C inside a ventilated oven until a constant mass was reached. Afterwards, they were kept in a desiccator until they achieved the room temperature and their dry mass (m_d) was obtained. Secondly, the specimens were forcibly-saturated under vacuum conditions until they reached a constant mass, obtaining the m_{Svac}. Subsequently, the saturated samples were put in a ventilated oven at 50 °C and the timer was started. At certain time intervals, initially short and then longer, the specimens were removed from the oven, weighed immediately (m_t) and then reintroduced into the oven. The time intervals between each weighing were 5 min in the range from 0 to 10 min, 10 min in the range from 10 min to 3 h, 20 min in the range from 3 to 6 h, and 0.5 h from 6 h to the obtainment of constant mass of the sample. Lastly, the S_r associated to each drying time was calculated through the Eq. (2).

After defining the relationship between the drying time and the S_r value reached for each tested calcarenite, the time needed to obtain S_r values of 25, 50 and 75% was determined by interpolation. Later, these estimations were used to prepare calcarenite specimens with these moisture values with the aim to carry out the mechanical tests.

2.3. Determination of the water distribution inside rock materials using MRI technique

The presence of water inside rock specimens and its distribution can

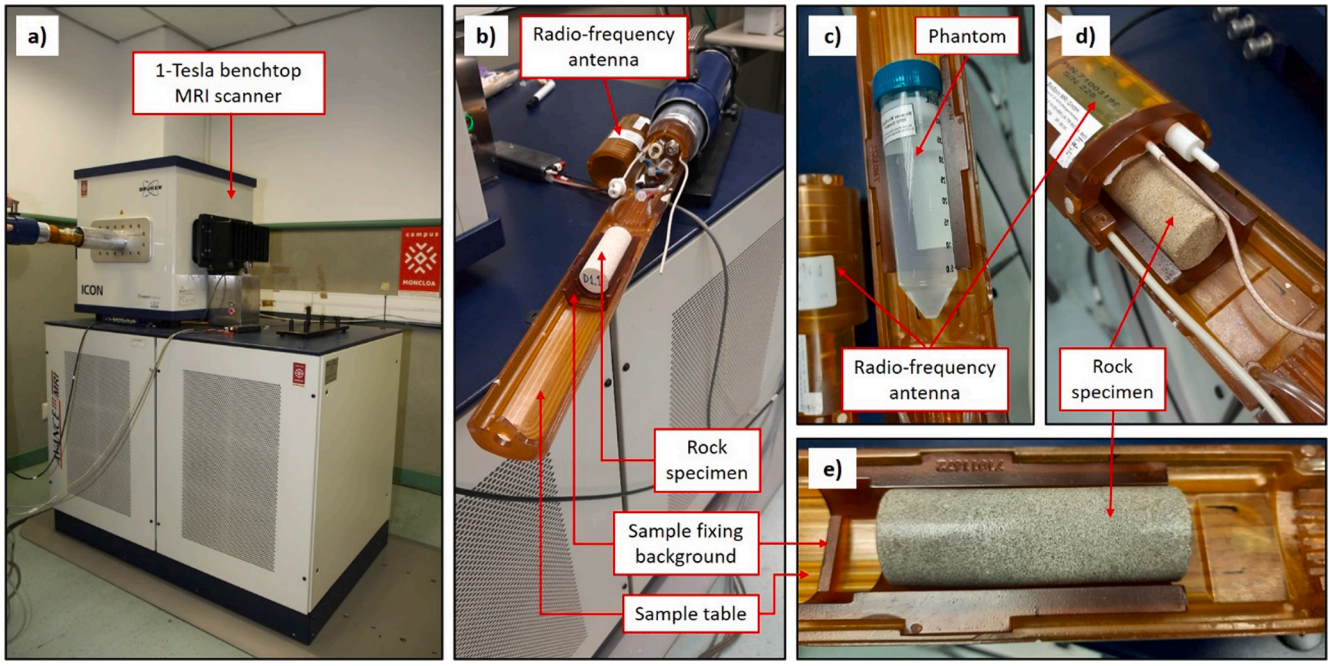

Fig. 1. Details of the MRI equipment used to determine the water distribution inside calcarenite specimens.

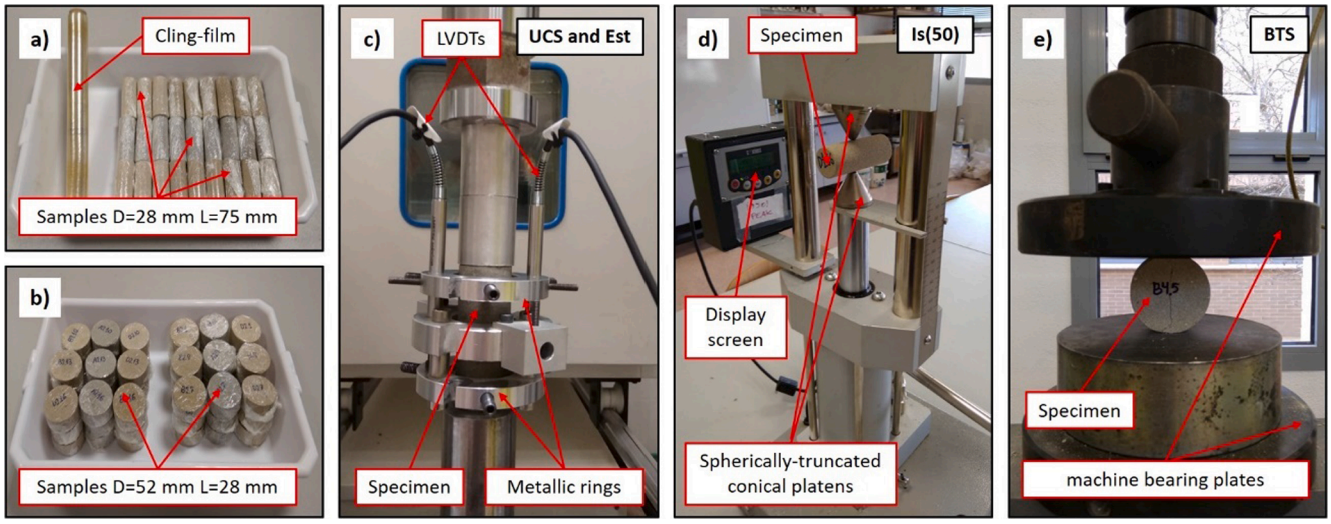

Fig. 2. Dimensions of specimens before mechanical tests (a and b) and equipment used in the UCS, E_{st} (c), $I_{s(50)}$ (d) and BTS (e) tests.

be obtained by using the Magnetic Resonance Imaging (MRI) technique. Particularly, this technique allows the detection of the hydrogen nuclei (protons, ^1H) of water and their corresponding energy states. ^1H possesses a property known as "spin", which can be comprehended as the nucleus spinning around its own axis. Due to its positive charge and spin property, hydrogen nuclei behave as small magnetic dipoles that are usually randomly oriented in all spatial directions but that can be properly magnetically excited to achieve valuable information. The implementation of the MRI technique to obtain the water distribution inside rock samples includes several phases. Firstly, a strong external magnetic field (B_o) is applied to the wet specimen in order to align the hydrogen nucleus in parallel with this external field. Then, a second radiofrequency (RF) magnetic field (B_1) is applied in short-duration pulses (microseconds) and in perpendicular direction to B_o. Thirdly, the energy absorbed and emitted by protons due to the transition from lesser to higher energy levels and vice-versa (on excitation and relaxation processes, respectively) induces a voltage that is detected by a coil of wire, amplified and showed as the "free-induction decay" (FID). Later, the FDIs obtained after applying several B_1 pulses are averaged to improve the time-domain signal. Finally, the signal-averaged FID is resolved using Fourier transformation process into and image, providing indirectly the water molecules location [68].

MRI tests were performed at the Bioimaging Center of the Complutense University of Madrid using a 1-Tesla benchtop MRI scanner [Icon (1 T-MRI); Bruker BioSpin GmbH, Ettlingen, Germany]. MRI spectrometer consists of a 1 T permanent magnet (without extra cooling required for the magnet) with a gradient coil that provides a gradient strength of 450 mT/m. An oval-cylinder solenoid radiofrequency coil (59×50 mm^2) was used. Details of the MRI equipment used are shown in Fig. 1. The main MRI experiment employed to monitor immersion and drying processes consisted of three-dimensional spin echo T1-weighted coronal images. The main selected parameters were: a repetition time of 500 ms, an echo time of 4.7 ms and a field of view of $40 \times 94 \times 40$ mm^3. The acquired matrix-size was $38 \times 142 \times 19$ and the reconstructed

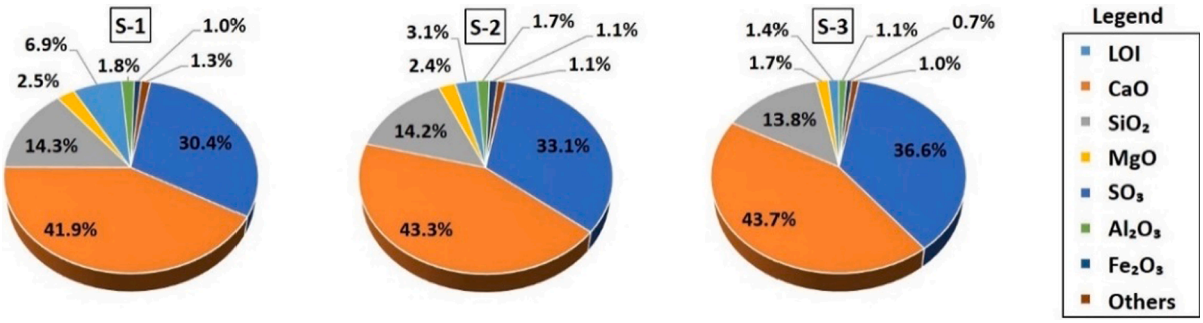

Fig. 3. Chemical composition (% Oxides) of the tested rocks obtained by XRF technique.

matrix-size 50 × 188 × 25 (resolution 0.80 mm × 0.50 mm × 1.60 mm). The total experiment acquisition time was approximately 6 min. All MRI data were acquired and analyzed using the software ParaVision 6.0.1 (Bruker, Ettlingen, Germany).

2.4. Determination of mechanical properties

With the aim to perform the UCS and E_{st} tests, a total of 90 specimens of 28 mm in diameter and 70–75 mm in length (30 units of each calcarenite variety) were prepared with different water contents. Specifically, half of the specimens of each variety (15 units) were wetted using the immersion procedure and the other half using the drying procedure. That is, three specimens for each S_r value (0, 25, 50, 75 and 100%) and for each partial water saturation process were prepared. These mechanical tests were carried out using a servo-controlled testing machine with a capacity of 200 kN and following the corresponding ISRM Suggested Methods [69]. In particular, sample strain was obtained using an instrument formed by two linked metallic rings located in parallel along the sample axis and two diametrically opposed Linear Variable Differential Transformers (LVDTs) that register changes in the axial relative distance between rings during unloading–reloading cycles (Fig. 2c). Axial strain was measured up to a maximum value equal to 40–50% of the ultimate load of samples to estimate the secant E_{st}. Once the E_{st} test was finished, the rings were removed from the specimen and the loading tests were repeated until failure. The used loading rate was 40 N/s. This value was chosen to ensure that the failure of most of the specimens occurred between 5 and 10 min after the start of the test according to the ISRM protocol [69]. This information is relevant in this research since the presence of water can rise the efficiency of time-dependent deformation mechanisms (e.g., stress corrosion cracking) in porous limestone [70,71].

For Point Load tests, 60 cylindrical specimens of 28 mm in diameter

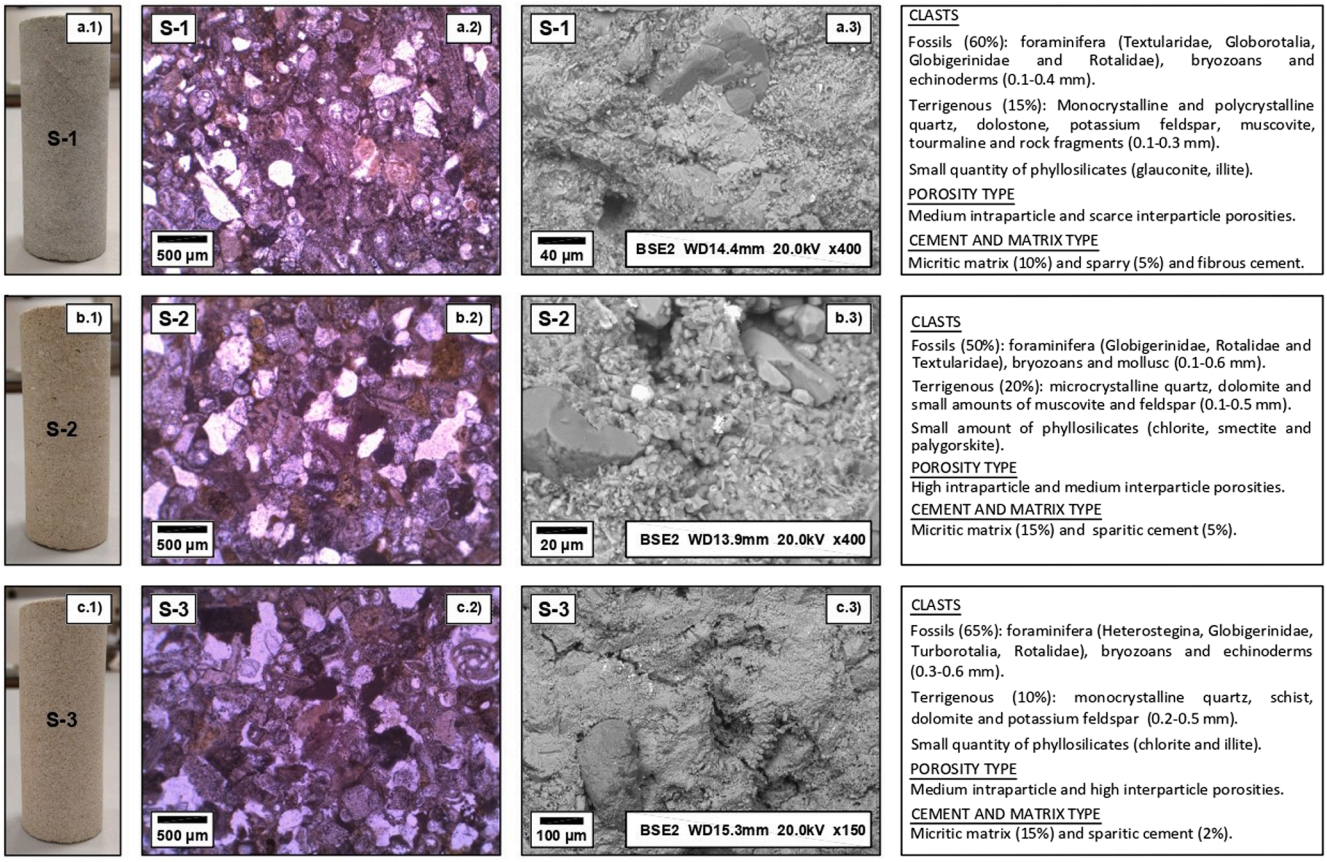

Fig. 4. Cylindrical specimens (a.1, b.1 and c.1), thin section microphotographs taken with parallel nicols (a.2, b.2 and c.2) and SEM images (a.3, b.3 and c.3) of the tested rocks.

of each calcarenite variety were used. Half of them were moistened with S_r values of 0, 25, 50, 75 and 100% through the water-immersion procedure and the other half were moistened with the same water content through the drying procedure (i.e, six units for each water content and each wetting process). The rock samples were diametrically loaded until failure applying a concentrated load by means of two spherically-truncated conical platens (Fig. 2d). As established in the corresponding ISRM suggested method [72], the load was gradually increased in order to ensure that the failure occurred between 10 and 60 s after the start of the test. $I_{s(50)}$ (MPa) was obtained using the Eq. (3):

$$I_{S(50)} = F \cdot I_S = \left(\frac{D}{50}\right)^{0.45} \cdot \frac{P}{D^2} \quad (3)$$

Where F is the size correction factor, I_s is the uncorrected Point Load Strength (MPa), P (N) is the ultimate load and D (mm) is the diameter of rock sample.

In the same way as for the compressive tests, 30 circular disks of 52 mm in diameter and 26–28 mm in thickness of each stone variety were made to perform BTS tests. Half of them were moistened with S_r values of 0, 25, 50, 75 and 100% through the water-immersion procedure while the other half were moistened with the same water content through the drying procedure (i.e., 3 units for each water content and each wetting process were tested). Due to the geometric differences between these samples and those used for the UCS and point-load experiments, the immersion and drying times required to reach the target S_r values in this type of specimens were adequately re-estimated before preparing the wet samples for the BTS tests. According to ASTM standard [73], the specimens were positioned in direct contact with the machine bearing plates during the tests and the load on the samples was continuously exerted at a constant rate such that ultimate load in the weakest rock materials occurs among 15 and 30 s after the start of the test (Fig. 2e). BTS (MPa) was obtained using the equation Eq. (4).

$$BTS = \frac{2 \cdot P}{\pi \cdot D \cdot L} \quad (4)$$

Where P is the maximum applied load indicated by the testing machine (N), L is the thickness of sample (mm) and D is its diameter (mm).

All mechanical tests were performed almost immediately after preparing the specimens with the corresponding water content. Specifically, the time elapsed between the wetting of each specimen and the start of the corresponding mechanical test varied between 5 and 10 min in order to ensure that water content and pore water distribution did not change significantly between both actions. Furthermore, in this short period of time between the wetting process and mechanical testing, samples were covered with a cling-film with the purpose of preserving their moisture (Fig. 2a and b).

3. Results and analysis

3.1. Mineralogical, chemical and physical properties

XRD analyses indicated that the rock materials used in this study are three limestone varieties mainly composed of calcite (70–80%), dolomite (5–10%), quartz (5–15%) and smaller quantities of feldspar, ankerite and phyllosilicates (5–10%). In line with this, XRF analyses showed that the most abundant chemical compounds of these materials (expressed as % oxides) are CaO (41.9–43.7%), SiO_2 (13.8–14.3%), SO_3 (1.4–6.9%), MgO (1.7–2.5%), Al_2O_3 (1.1–1.8%), Fe_2O_3 (0.7–1.1%) and K_2O (0.5–0.6), apart from the loss on ignition (LOI). Chemical analysis of each calcarenite variety is shown in Fig. 3.

According to Ordoñez et al. [74], tested rocks are composed of primary sediments that belong to the continental shelf with discontinuous deposition characterized by erosional unconformities and rough waters in which the presence of planktonic, nektonic and benthic organisms is common and causes reworking and movement of sediments. Therefore, these sedimentary rocks frequently exhibit large quantities of organic shells and bioturbation. From a petrological point of view, the three studied stones are allochemical calcareous materials (fine- and medium-grained biocalcarenites) principally constituted of fossils and different amounts of fragmentary quartz [75]. Particularly, a mean grain size of 0.2 mm was observed in S-1, 0.3 mm in S-2 and 0.4 mm in S-3. Thin section microphotographs, SEM images and petrographic descriptions of each tested calcarenite can be seen in Fig. 4.

Table 2
Physical properties of the tested rocks.

	S-1	S-2	S-3
Dry density, ρ_{dry} (g/cm^3)	2.30 ± 0.01	2.17 ± 0.01	2.11 ± 0.01
Saturated density, ρ_{sat} (g/cm^3)	2.40 ± 0.01	2.34 ± 0.01	2.31 ± 0.01
Particle density, ρ_t (g/cm^3)	2.68 ± 0.01	2.71 ± 0.01	2.70 ± 0.01
Open porosity, p_o (%)	11.59 ± 0.24	17.99 ± 0.42	20.45 ± 0.36
Total porosity, p (%)	15.00 ± 0.25	20.05 ± 0.41	21.94 ± 0.44
Water absorption, W_a (%)	5.05 ± 0.11	8.27 ± 0.22	9.65 ± 0.22
P-wave velocity, v_p (km/s)	4.55 ± 0.08	3.39 ± 0.10	4.16 ± 0.04
S-wave velocity, v_s (km/s)	2.63 ± 0.07	2.06 ± 0.06	2.42 ± 0.07
Water absorption coefficient by capillarity, C (g/m^2·s$^{0.5}$)	12.67 ± 0.62	11.52 ± 1.33	51.29 ± 3.44
Water permeability, k (mD)			
θ = 0°	4.76 · 10^{-4}	8.87 · 10^{-4}	6.63 · 10^{-2}
θ = 45°	6.73 · 10^{-4}	1.25 · 10^{-3}	9.37 · 10^{-2}
θ = 80°	2.74 · 10^{-3}	5.11 · 10^{-3}	0.382
Pore throat size distribution (%)			
<0.01 μm	7.79	2.03	2.71
0.01–0.1 μm	25.28	10.98	7.92
0.1–1 μm	52.88	42.89	24.17
1–10 μm	5.86	35.16	50.35
10–100 μm	4.85	5.79	11.23
>100 μm	3.34	3.15	3.61
Specific Surface Area (m^2/g)	5.54	3.17	3.23
Total interparticle porosity (%)	1.46	2.79	8.30
Total intraparticle porosity (%)	11.86	15.90	12.18
Total porosity MIP (%)	13.32	18.69	20.48
Pore Tortuosity	2.09	2.03	2.01
Fractal Dimension			
Intrusion	3.07	2.80	3.02
Extrusion	2.83	1.94	2.25

Concerning the physical properties of studied calcarenites, ρ_{dry} and ρ_{sat} ranged from 2.11 to 2.30 g/cm^3 and from 2.31 to 2.40 g/cm^3, respectively. Specifically, the highest values were obtained in S-1 while the lowest values were found in the S-3. Accordingly, S-1 exhibited the smallest values of p_o, p and W_a (11.59, 15.00 and 5.05% respectively) while S-3 showed the greatest values (20.45, 21.94 and 9.65%, respectively). Regarding v_P and v_S, the highest values were measured in S-1 (4.55 km/s and 2.63 km/s, respectively) and the lowest values were found in S-2 (3.39 km/s and 2.06 km/s, respectively). With respect to the porous structure, the lowest pore throat size and the highest specific surface area and tortuosity values were found in S-1, while S-2 and S-3 exhibited similar values each other. Furthermore, the highest value of interparticle porosity was found in S-3 while the greatest intraparticle porosity was measured in S-2. The physical properties of the studied rocks are summarized in Table 2 and a comparison of the pore throat size distribution of each material obtained through the MIP technique is shown in Fig. 5.

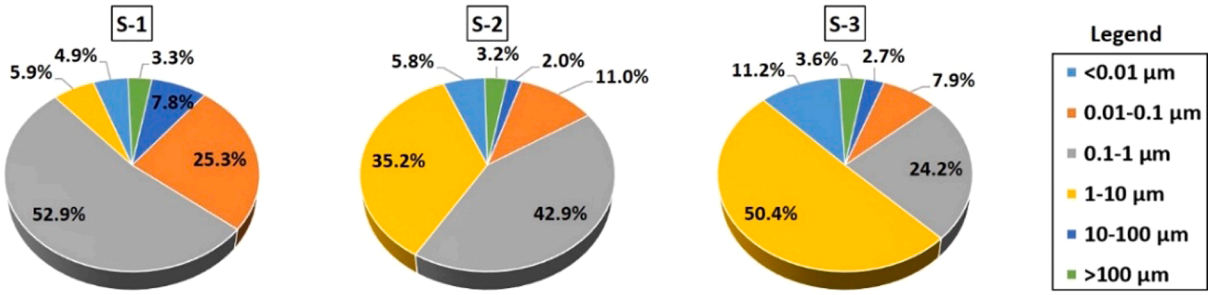

Fig. 5. Comparison of the pore throat size distribution of the three rocks obtained by using MIP technique.

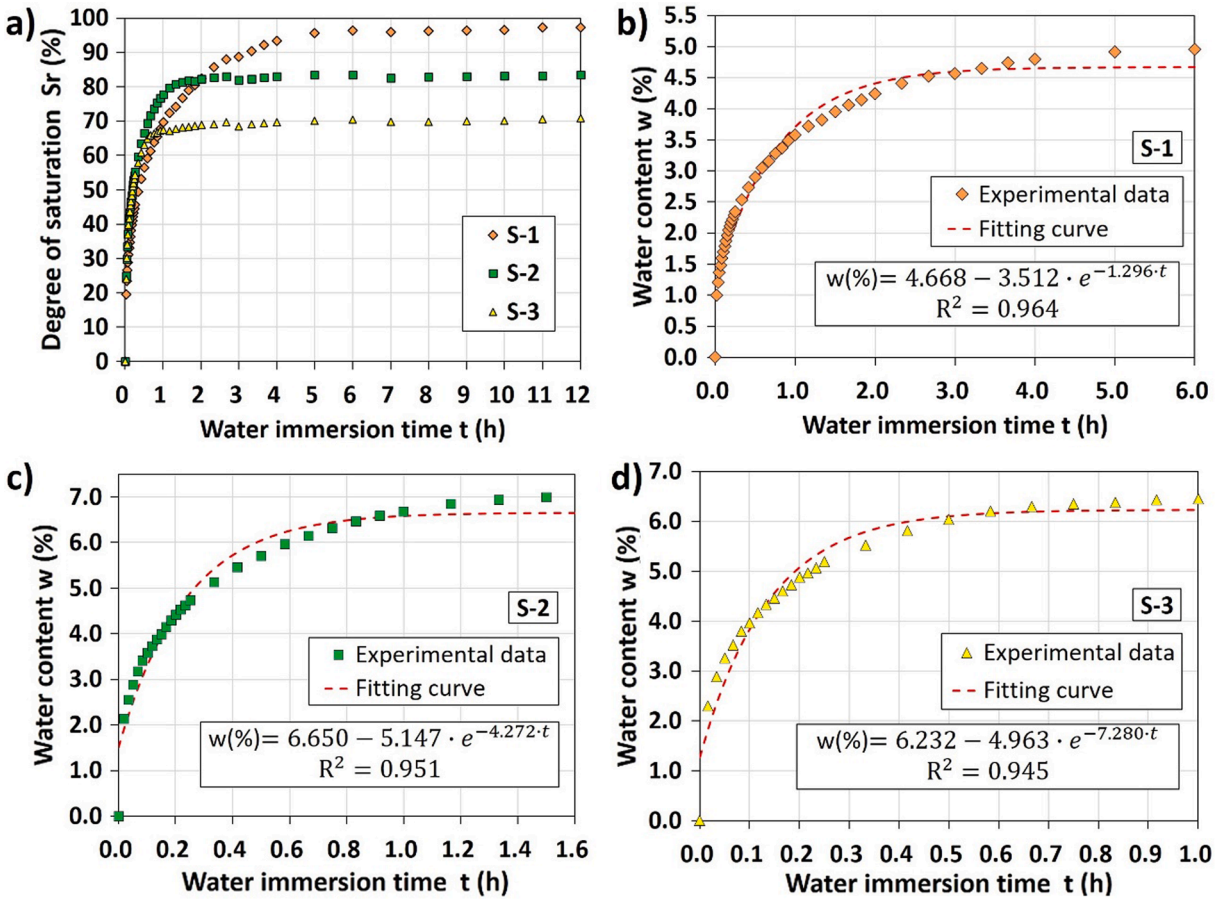

Fig. 6. Variation of degree of saturation (S_r) (a) and water content (w) (b, c and d) with water-immersion time (t) for 28 mm-diameter samples of the three tested rocks.

3.2. Variation of moisture content and water distribution with immersion time

The partial saturation procedure consisting in submerging rock specimens in water under atmospheric pressure during different time intervals allows to easily obtain S_r values ranging between 25 and 70–75% in the three calcarenite varieties. Specifically, the S_r values reached after one minute of water immersion were 19.5, 24.9, 24.1 for S-1, S-2 and S-3, respectively. On the other hand, the maximum values of S_r obtained were 96.5, 83.2 and 70.5 for S-1, S-2 and S-3, respectively. They were reached for immersion times equal to or less than eight hours. This indicates that pores are not fully saturated at atmospheric pressure regardless of the immersion time at which rock specimens are exposed and that, therefore, the use of a vacuum pump is required to obtain fully water saturation specimens (S_r = 100%).

In this water saturation process of 28 mm-diameter samples, three clearly differentiated stages can be distinguished (Fig. 6a): a first stage in which the relationship between the immersion time and the S_r reached is quasi-linear; a second transition stage in which the saturation rate is slowly decreasing and the data could be fitted to a convex curve; and a third stage that can be represented with a horizontal line due to the S_r has reached its maximum value and remains constant regardless of the immersion time. The relationship between the immersion time and the water content absorbed by the rocks has been modelled by using exponential fitting functions, which allows estimating the time required to achieve a specific w or S_r value for each calcarenite variety (Fig. 6b, 6c and 6d).

Cross and longitudinal section images obtained through MRI technique show the water distribution inside each calcarenite variety after immersing them in water during different time intervals (Fig. 7). These

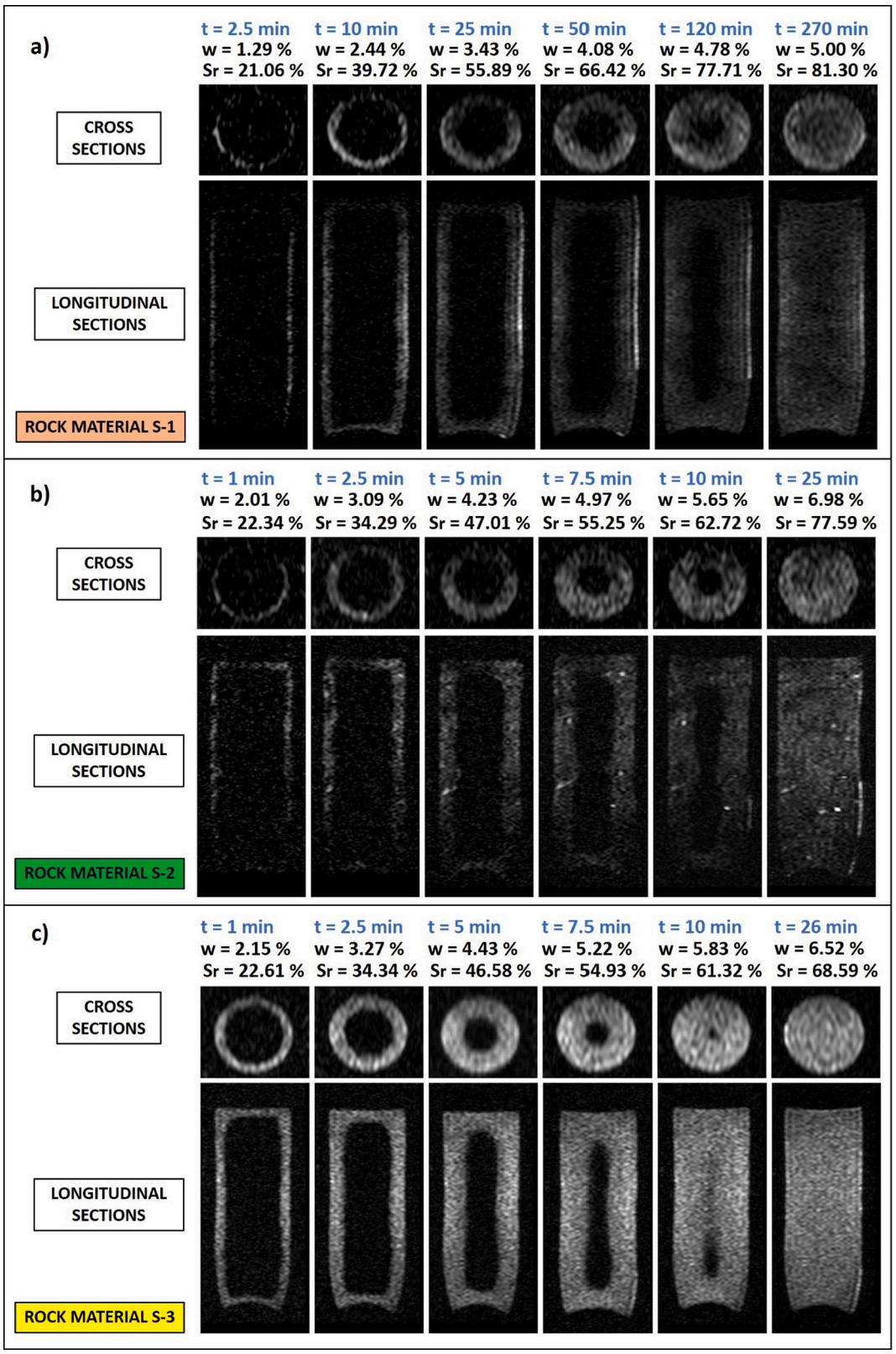

Fig. 7. Cross and longitudinal section images obtained through MRI technique that show the water distribution inside each calcarenite variety after immersing them in water during different time intervals. Cross and longitudinal sections were taken at the mid-point of the length and the centre of the bases of specimens, respectively.

images demonstrate that water distribution inside pore network of these materials moistened using this wetting procedure is not uniform. That is, initially, when the specimens start to soaked, water is only localised on the outer zone of the sample while the inner zone remains in dry state. Then, when the immersion time increases, water penetrates continuously into the pores and a wet ring with a thickness that grows

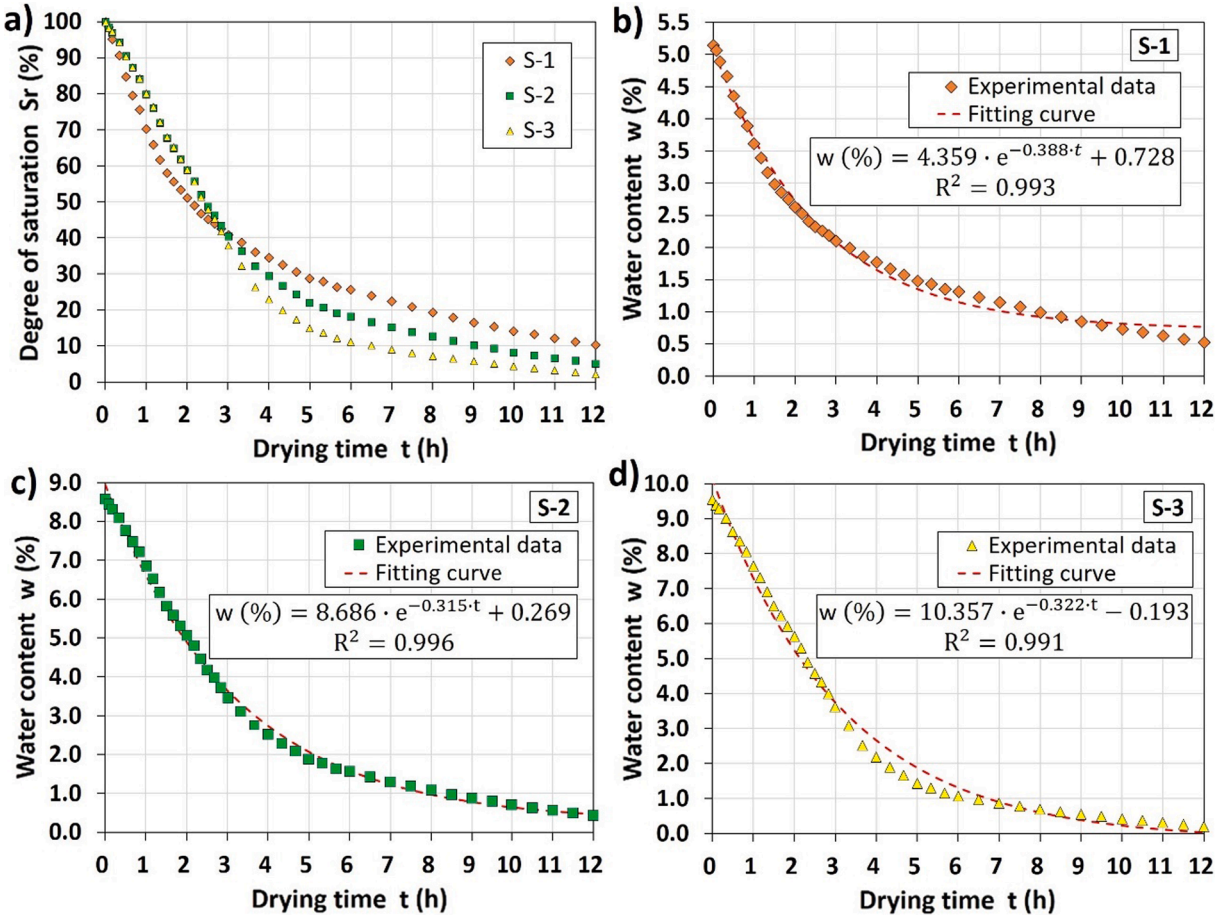

Fig. 8. Variation of degree of saturation (S_r) (a) and water content (w) (b, c and d) with drying time (t) for 28 mm-diameter samples of the three tested rocks.

progressively is observed. Finally, water fills the entirely of the specimens and they reach their maximum S_r value at atmospheric pressure. Although the form in which water is distributed inside the specimens when time increases is quite similar for the three calcarenite varieties, the accessing velocity of water is significantly dissimilar. In this sense, the immersion time required for water to achieve the longitudinal axis of specimens was considerably longer in S-1 (around 4.5 h) in comparison with the time needed in the other varieties (around 25 min in S-2 and 15 min in S-3). This can be explained by the fact that S-1 presents pore throat diameters substantially smaller than the other calcarenites and also a greater tortuosity, which hampers water penetration.

3.3. Variation of moisture content and water distribution with drying time

The oven drying procedure of saturated samples at 50 °C during different time intervals allows to obtain rock specimens with S_r values ranging between 10 and 100% for all the three studied calcarenites in drying time<12 h. The porous structure of these rock material moderately influences the drying process. In particular, S-1 needed drying times higher than S-2 and S-3 to obtain small values of S_r due to its lower pore throat size and its greater tortuosity (Fig. 8a).

In this drying process of 28 mm-diameter samples, three stages can be distinguished: a first stage in which the relationship between the drying time and the obtained S_r value is nearly linear; a second transition stage in which the drying rate decreases gradually and the data takes the form of a concave curve; and a third stage in which the drying speed is very small and the relationship between the S_r and the drying time becomes linear again. This process can be modelled through decreasing exponential fitting functions that allows estimating the time required to reach a specific w or S_r value in each calcarenite variety (Fig. 8b, 8c and 8d).

Cross and longitudinal section images obtained through MRI technique show the water distribution inside each calcarenite variety after drying them in an oven at 50 °C during different periods of time (Fig. 9). These images reveal that, at the beginning of the drying process, the water localised on the outer zone of the samples is progressively evaporated while the inner zone remains in wet state. Then, when the drying time increases, innermost water disappears gradually and, finally, specimens are completely dry. In addition, water molecules of partial saturated specimens prepared using this procedure are generally distributed in a more homogeneous way and in a larger region of the sample in comparison with the water molecules of the partial saturated specimens prepared using the immersion process.

3.4. Relationships between water content and compressive properties (UCS and E_{st}) of calcarenites

The values of the compressive parameters (UCS and E_{st}) for water contents associated with S_r values of 0, 25, 50, 75 and 100% and obtained from both wetting procedures (immersion and drying processes) in the three tested calcarenites are shown in Figs. 10 and 11. Generally, UCS and E_{st} decreased when water content increased for both procedures and all tested rocks. Specifically, when water content in S-1 increased from 0.0 to 5.0%, the UCS decreased from 40.1 to 18.7 MPa and the E_{st} reduced from 25.6 to 11.8 GPa. In S-2, when water content rose from 0.0 to 8.4%, UCS diminished from 22.6 to 8.2 MPa and E_{st} reduced from 8.1 to 2.5 GPa. Similarly, in S-3, when water content increased from 0.0 to 9.6%, UCS decreased from 27.2 to 18.9 MPa and E_{st} reduced from 20.5 to 15.4 GPa.

However, the evolution of UCS and E_{st} with S_r was slightly different

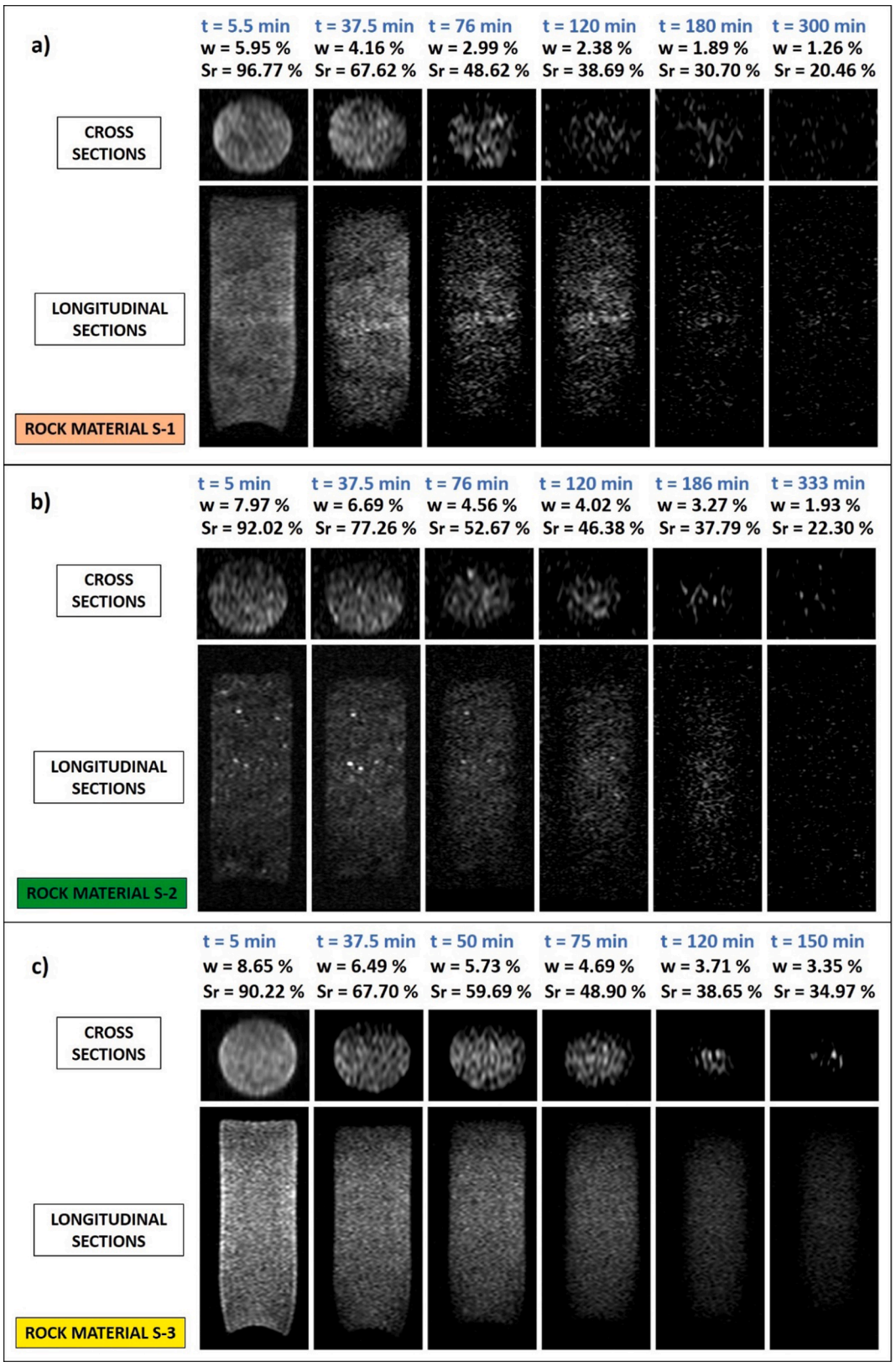

Fig. 9. Cross and longitudinal section images obtained through MRI technique that show the water distribution inside each calcarenite variety after drying them in an oven at 50 °C during different time intervals. Cross and longitudinal sections were taken at the mid-point of the length and the centre of the bases of specimens, respectively.

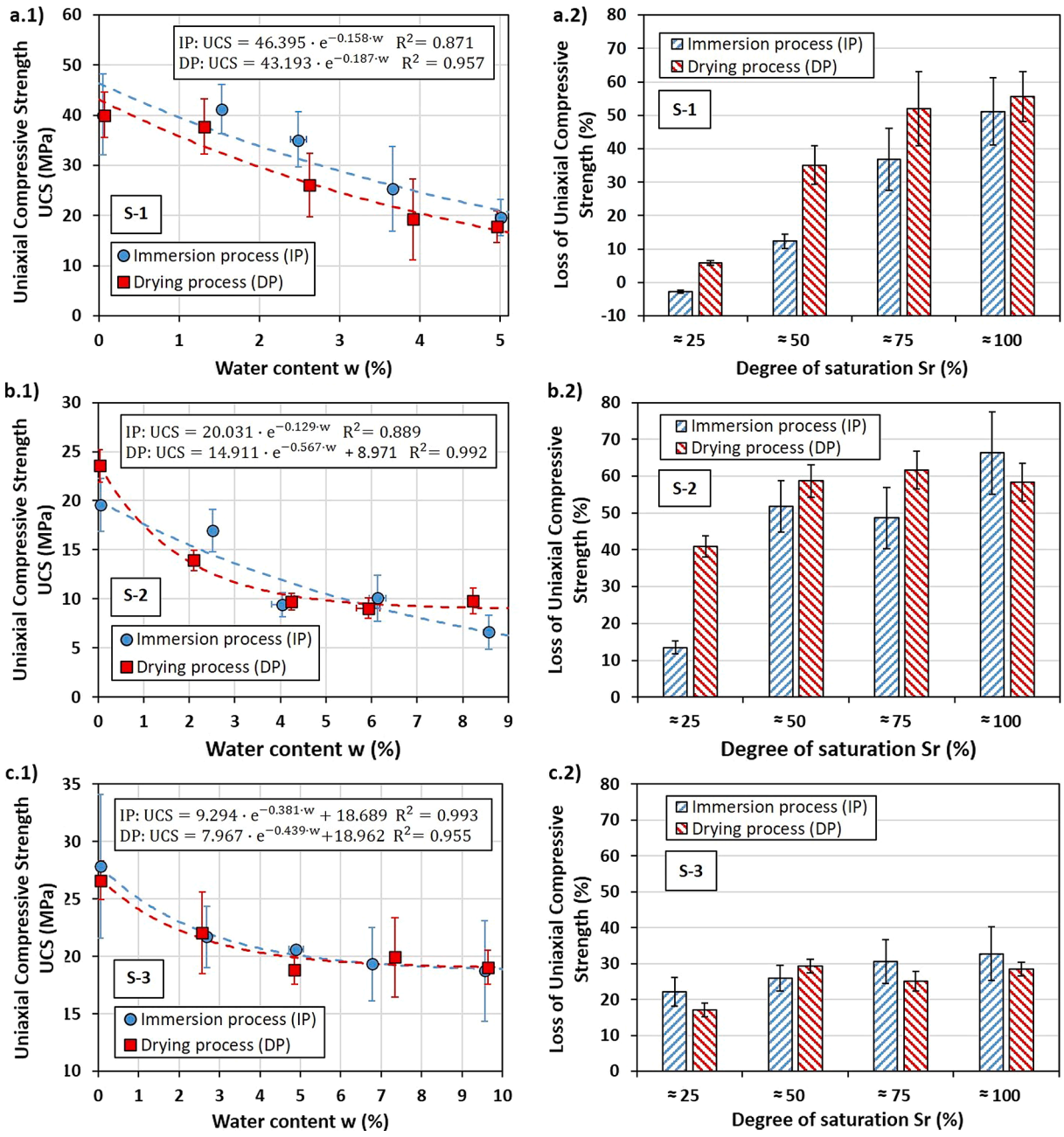

Fig. 10. Effect of moisture content (w) on Uniaxial Compressive Strength (UCS) for the three tested rocks depending on the water saturation procedure used. Left: Relationships between w and UCS (a.1, b.1 and c.1). Right: Losses of UCS for different S_r values (a.2, b.2 and c.2).

depending on the partial saturation procedure used. In this line, for small values of S_r (25 and 50%), the specimens moistened by the oven drying process frequently exhibited more marked decreases of these properties than the specimens wetted by the immersion procedure, while the value of these parameters were quite similar for higher values of S_r (≥75%) for both wetting procedures. This effect was especially marked in S-2, in which for S_r = 25% the UCS loss was 40.9% in the specimens moistened using the drying process while was 13.5% in the specimens wetted using the immersion process. In the same way, in this variety the E_{st} loss for S_r = 25% was 44.9% in the specimens wetted using the drying process while was 22.7% in the specimens wetted using the immersion procedure. (Figs. 10 and 11).

The quantitative relationships between the compressive properties (UCS and E_{st}) and the water content (w and S_r) were obtained by fitting each dataset (constituted by a calcarenite variety and a wetting procedure) to the following negative tri-parametric exponential function:

$$y = a \cdot e^{-bx} + c \tag{5}$$

where *y(x)* is the corresponding mechanical property, *x* is the water content *w* (or the degree of saturation S_r) and, *a*, *b* and *c* are three constants of the rock. This function type, which has been the most frequently used curve to describe the variation of mechanical parameters with moisture, allows to express the mechanical values at cero water content as *a* + *c*, the mechanical values at high water content (completely saturated condition) as *c* and the rate of the mechanical property reduction with increasing water content as *b* [50,55,76]. Generally, this function type fitted quite well to all datasets. Nevertheless, for S-1 and for the specimens of S-2 wetted using the immersion process the parameter *c* was set at zero and only the parameters *a* and *b*

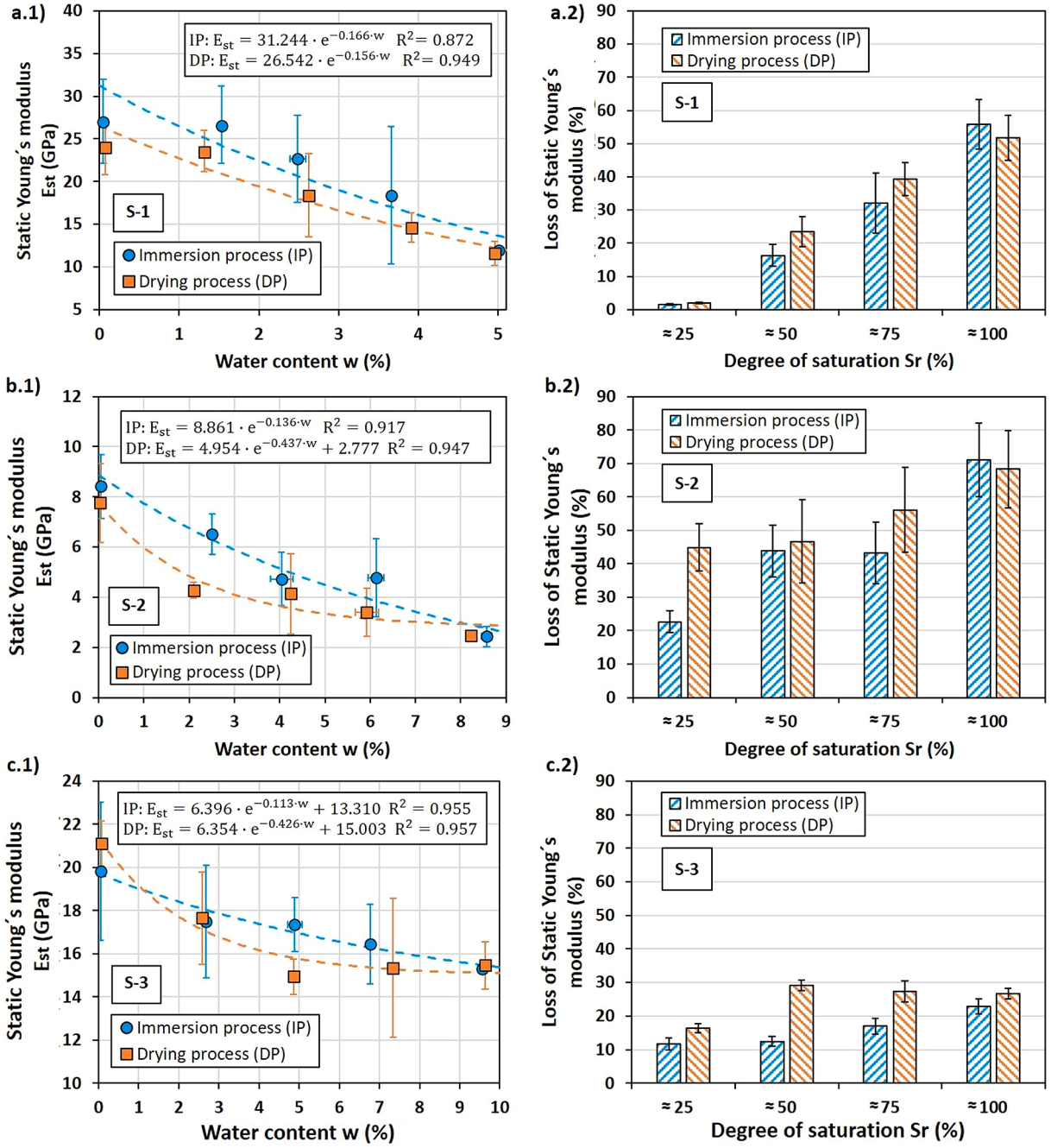

Fig. 11. Effect of moisture content (w) on Static Young's modulus (E_{st}) for the three tested rocks depending on the water saturation procedure used. Left: Relationships between w and E_{st} (a.1, b.1 and c.1). Right: Losses of E_{st} for different S_r values (a.2, b.2 and c.2).

were calculated due to data representation indicated that the variations of compressive parameters with water content were more gradual in these cases (Table 3).

3.5. Relationships between water content and tensile properties (BTS and $I_{s(50)}$) of calcarenites

The values of tensile properties ($I_{s(50)}$ and BTS) for water contents associated with S_r values of 0, 25, 50, 75 and 100% and obtained from both partial water saturation procedures in the tested stones are reflected in Figs. 12 and 13, respectively. Generally, these tensile properties decreased when the S_r increased.

With regard to $I_{s(50)}$, it diminished from 3.9 to 1.9 MPa in S-1, from 1.8 to 0.8 MPa in S-2, and from 2.8 to 1.8 in S-3 when the S_r was increased from 0 to 100%. However, it was found that the evolution of $I_{s(50)}$ with the water content was greatly influenced by the partial saturation procedure used. In this connection, for the same value of S_r, the specimens wetted using the immersion procedure commonly exhibited smaller decreases of $I_{s(50)}$ than the specimens moistened through the oven drying process in all tested calcarenite varieties. Particularly, when S_r = 25%, the value pairs of the reductions of $I_{s(50)}$ (immersion process–drying process) were 9.9–41.7% in S-1, 22.8–45.7% in S-2, and 11.9–26.4% in S-3; when S_r = 50%, the decreases of $I_{s(50)}$ were 23.2–53.5% in S-1, 42.7–55.8% in S-2, and 22.2–34.7% in S-3; and when S_r = 75%, the reductions of $I_{s(50)}$ were 38.7–53.9% in S-1, 51.5–58.8% in S-2, and 26.5–35.3% in S-3 (Fig. 12). As a consequence, b-parameters of the exponential fitting functions that correlate water content and $I_{s(50)}$ were very different depending on the wetting process used for the three

Table 3
Equations correlating compressive properties (UCS and E_{st}) and water content (w and S_r) in the tested rocks depending on the wetting procedure used.

Wetting procedure	Rock material		
	S-1	S-2	S-3
Immersion process	$UCS = 46.40 \cdot e^{-0.158w}$ $R^2 = 0.871$	$UCS = 20.03 \cdot e^{-0.129w}$ $R^2 = 0.889$	$UCS = 9.29 \cdot e^{-0.381w} + 18.69$ $R^2 = 0.993$
	$E_{st} = 31.24 \cdot e^{-0.166w}$ $R^2 = 0.872$	$E_{st} = 8.86 \cdot e^{-0.136w}$ $R^2 = 0.917$	$E_{st} = 6.40 \cdot e^{-0.113w} + 13.31$ $R^2 = 0.955$
	$UCS = 46.36 \cdot e^{-0.0079S_r}$ $R^2 = 0.874$	$UCS = 20.15 \cdot e^{-0.0109S_r}$ $R^2 = 0.882$	$UCS = 9.31 \cdot e^{-0.0374S_r} + 18.69$ $R^2 = 0.993$
	$E_{st} = 31.19 \cdot e^{-0.0083S_r}$ $R^2 = 0.871$	$E_{st} = 8.87 \cdot e^{-0.0114S_r}$ $R^2 = 0.896$	$E_{st} = 6.23 \cdot e^{-0.0116S_r} + 13.49$ $R^2 = 0.958$
Oven drying process	$UCS = 43.19 \cdot e^{-0.187w}$ $R^2 = 0.957$	$UCS = 14.91 \cdot e^{-0.567w} + 8.97$ $R^2 = 0.992$	$UCS = 7.97 \cdot e^{-0.439w} + 18.96$ $R^2 = 0.955$
	$E_{st} = 26.54 \cdot e^{-0.156w}$ $R^2 = 0.949$	$E_{st} = 4.95 \cdot e^{-0.437w} + 2.78$ $R^2 = 0.947$	$E_{st} = 6.35 \cdot e^{-0.426w} + 15.00$ $R^2 = 0.957$
	$UCS = 43.14 \cdot e^{-0.0094S_r}$ $R^2 = 0.952$	$UCS = 14.95 \cdot e^{-0.0447S_r} + 8.92$ $R^2 = 0.991$	$UCS = 7.97 \cdot e^{-0.0435S_r} + 18.97$ $R^2 = 0.956$
	$E_{st} = 26.55 \cdot e^{-0.0079S_r}$ $R^2 = 0.949$	$E_{st} = 5.01 \cdot e^{-0.0339S_r} + 2.73$ $R^2 = 0.951$	$E_{st} = 6.35 \cdot e^{-0.0422S_r} + 15.01$ $R^2 = 0.958$

rocks (Table 4).

Concerning the BTS, it reduced from 6.6 to 3.4 MPa in S-1, from 4.2 to 1.8 MPa in S-2, and from 4.9 to 2.7 in S-3 when S_r increased from 0 to 100%. Furthermore, slightly different behaviours regarding the variation of this property with water content were found depending on the rock material and the wetting procedure used. In this sense, in S-1, for small values of S_r (25%), the specimens moistened using the oven drying process exhibited higher decreases of BTS (a drop of 27.1%) than the specimens wetting through the immersion procedure (a drop of 13.1%), while for greater S_r values the reductions of BTS were quite similar for both processes (drops of 34.6–37.1% for $S_r = 50\%$ and of 44.9–37.0% for $S_r = 75\%$). In addition, in S-2 and S-3, the reductions of BTS were very close for both partial saturation procedures and for all S_r values (Fig. 13). The tri-parametric negative exponential functions correlating water content (w or S_r) and BTS for each calcarenite variety and each wetting procedure can be seen in Table 4.

3.6. Failure pattern of specimens

Failure modes of calcarenite specimens prepared with different water contents (S_r values of 0, 25, 50, 75 and 100%) under uniaxial compression and moistened through immersion and drying processes are shown in Fig. 14. Generally, dry specimens exhibited cracks both on the surface and in the inner zones and the most common failure pattern observed in them was axial splitting. Despite this, shear failure with small zones of mixed tensile-shear cracks were also detected in some dry samples (especially in S-2). On the contrary, fully saturated specimens mainly exhibited shear-dominated failure, although small regions with cracks associated to axial splitting were also observed in some samples (especially in S-1).

Regarding partially water-saturated samples, slight differences were detected depending on the wetting procedure used. On the one hand, specimens wetted through the immersion process and with small S_r values (25 and 50%) principally showed splitting failure with tensile-dominated cracks. Nevertheless, few specimens of S-1 and S-3 also displayed signs of both splitting and shear failure. Furthermore, cracks were predominantly accumulated near the surface of samples where the water was accumulated (important reduction of mechanical properties occurs in this zone) while the inner zone of specimens remained intact and in dry state). In this connection, as pointed out by Tang [55], the axial splitting failure pattern observed in this case could be related to the difference of lateral deformability among the wet and dry areas, which may cause tensile stress at the interface between both regions. For higher S_r values (75%), S-2 frequently showed shear-dominate failure while S-1 and S-3 exhibited commonly splitting or mixed tensile-shear failure. On the other hand, specimens partially water-saturated through the drying procedure mostly showed axial splitting failure in the three calcarenites, although scarce specimens of S-2 exhibited shear-dominate or mixed tensile-shear failure. The more consistent and homogeneous failure modes observed in this case might be due to the fact that the water inside the specimens was distributed in a wider region of the cross section. In any case, the failure pattern of rocks under uniaxial compression is a complex issue which depends on several aspects and, therefore, further investigations on this topic will be required.

Typical failure modes obtained in the BTS tests for calcarenite specimens prepared with different water contents (S_r values of 0, 25, 50, 75 and 100%) by using both immersion and drying processes are shown in Fig. 15. In the three varieties and for all water contents and both wetting procedures the observed failure patterns were fractures practically parallel to the loading direction and situated in the central part (i.e., located inside the region defined by 10% of the diameter of the specimens on both sides of the imaginary line joining the contact areas between the sample and the bearing plates). Additionally, during the BTS tests, it was detected that as water content increased, the specimens exhibited lower disintegration and their cracking sounds were less intense. Also, for the same and small S_r values ($\leq$50%), the specimens moistened using the drying process displayed a softer and a more gradual failure than those wetted using the immersion process.

Failure patterns of specimens obtained in diametral Point Load tests for tested calcarenites prepared with different moisture contents (S_r values of 0, 25, 50, 75 and 100%) by using the immersion and drying procedures are displayed in Fig. 16. The failure mode of the vast majority of specimens happened in a valid way according to ISRM Suggested Method [72]. However, an invalid failure pattern (fracture surface passed through only one point) was specifically obtained in some specimens of S-1 wetted with a S_r value of 25% by using the immersion process. This finding can be attributed to the more heterogeneous water distribution inside the specimens prepared using this procedure and the lower permeability of S-1 compared to the other varieties (due to its smaller porosity and pore throat size and its greater tortuosity). In other words, for this small moisture content and wetting process, water was especially concentrated in the outer zone in S-1 and, as a consequence, the external surface of specimens became the weakest region, which caused that cracks propagated toward this weak wet region rather than the dry strong region at the core of the specimens. Furthermore, it was observed that for the three calcarenite varieties and for S_r values lower than 50%, the specimens moistened using the drying process exhibited a softer failure than those wetted using the immersion process. Also, as pointed out for BTS test, the failure of specimens tested under diametral PLT occurred in a less abrupt manner when water content increased.

3.7. Influence of wetting procedure on the relationships between mechanical properties

Compressive properties such as UCS and E_{st} are the two most important mechanical properties of rock materials due to their obtainment is crucial for performing safety evaluations in several civil and mining works. Nevertheless, standard test for assessing these parameters are time-consuming, expensive and demand the use of heavy equipment [19,77]. Furthermore, in some cases such as weathered or weak rock

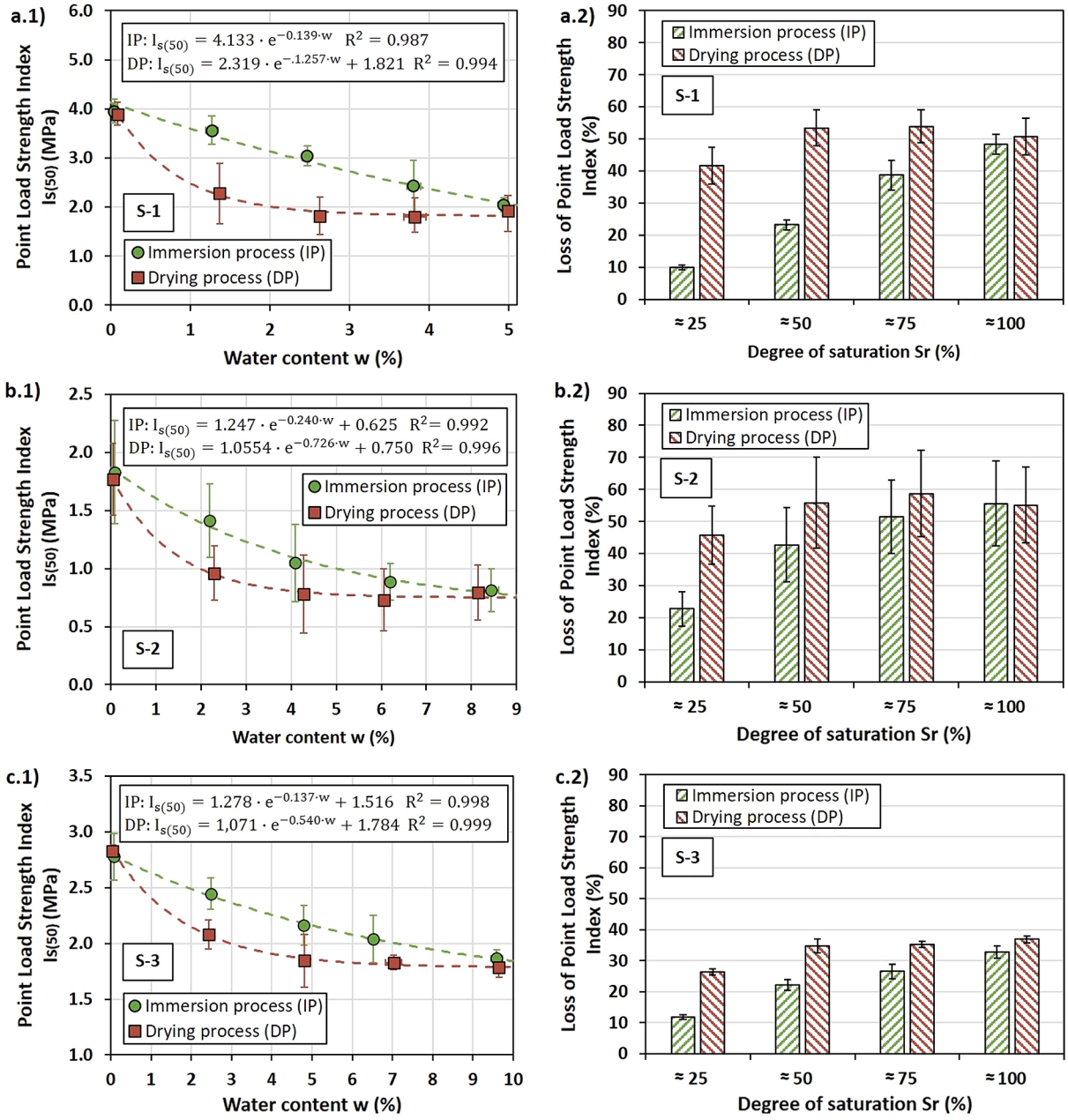

Fig. 12. Effect of moisture content (w) on Point Load Strength Index ($I_{s(50)}$) for the three tested rocks depending on the water saturation procedure used. Left: Relationships between w and $I_{s(50)}$ (a.1, b.1 and c.1). Right: Losses of $I_{s(50)}$ for different S_r values (a.2, b.2 and c.2).

materials, the preparation of specimens with the shape and size required by standards is tricky [78]. As a consequence, the indirect determination of these properties using functions that correlate these parameters with other faster and cheaper indexes such as $I_{s(50)}$ and BTS is very practical [26].

Previous works have already provided useful correlation functions between some of these mechanical properties and indexes for similar calcarenites [11]. However, this study goes far beyond that and assesses the effect of water distribution on these relationships by testing partially saturated specimens wetted through both the immersion and drying procedures and analyses them jointly and separately. The pair of mechanical values of each dataset and the obtained through-the-origin linear correlation functions are depicted in Fig. 17.

Generally, the ratios between the mechanical parameters slightly change depending on the used wetting procedure. In particular, the values of the slopes of the different through-the-origin linear fitting functions obtained for immersion and drying processes were: 10.4–11.3 for UCS/$I_{s(50)}$, 6.4–6.0 for UCS/BTS, 7.0–7.4 for $E_{st}/I_{s(50)}$, 4.3–3.8 for E_{st}/BTS, 0.7–0.6 for E_{st}/UCS and 1.6–1.9 for BTS/$I_{s(50)}$. From an engineering point of view, the choice of the correct value of the ratio to be used by the end-user requires knowledge of whether the rock mass or the building element made of stone is in the process of wetting or drying. To this aim, advanced monitoring systems, which can continuously record the temporal evolution of the water table of the rock mass or a continuous data record of rainfall, humidity and temperature in the surroundings of the stone construction element, are required. Therefore, in the case of large architectural and civil engineering projects where this information is available, an accurate indirect estimation of the strength and deformability of the rock material can be done. By contrast, in the case of modest works without this advanced monitoring, the corresponding smallest ratio value should be adopted in order to be conservative from a safety perspective.

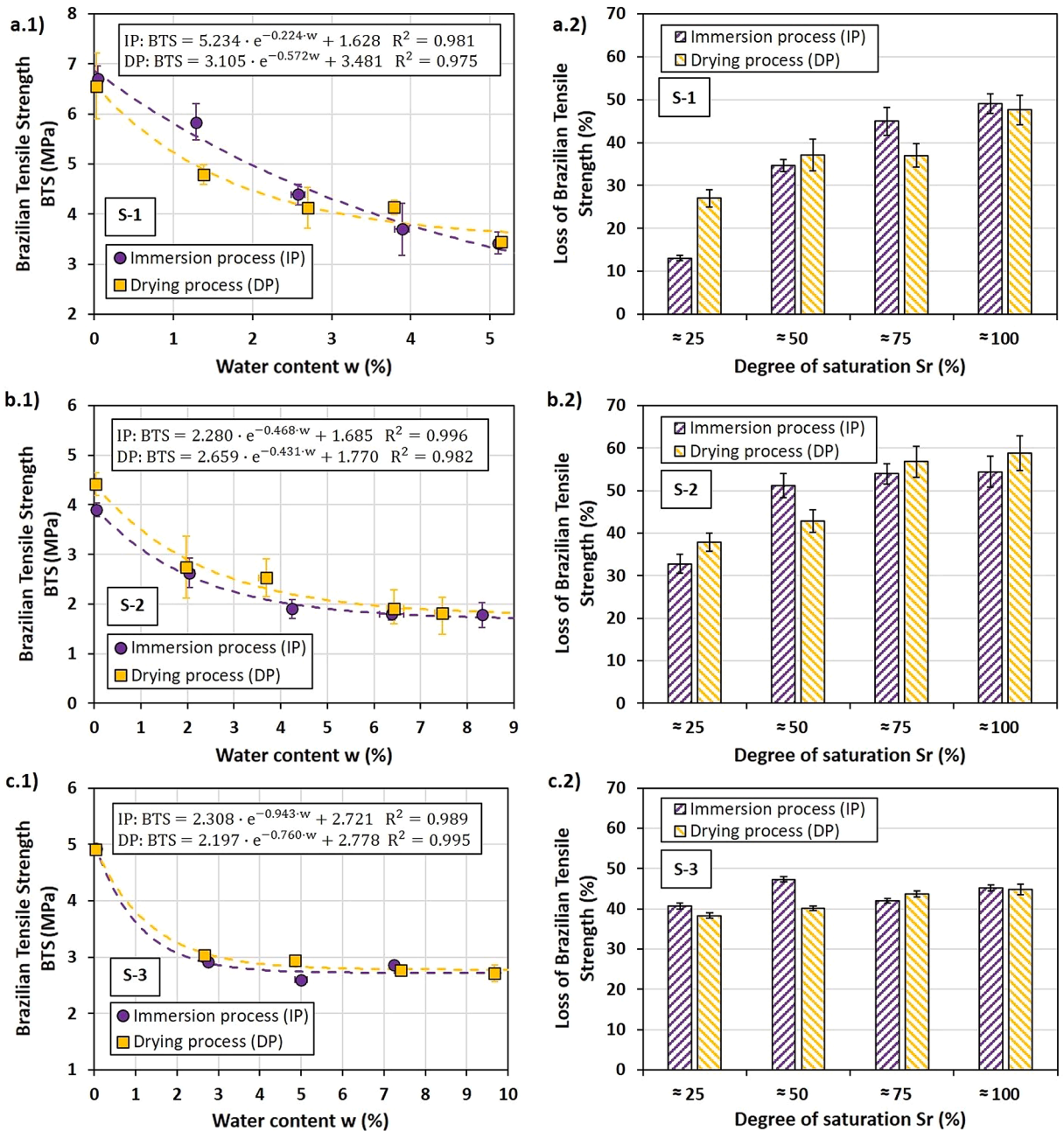

Fig. 13. Effect of moisture content (w) on Brazilian Tensile Strength (BTS) for the three tested rocks depending on the water saturation procedure used. Left: Relationships between w and BTS (a.1, b.1 and c.1). Right: Losses of BTS for different S_r values (a.2, b.2 and c.2).

4. Discussion

In this work, the influence of moisture content and water distribution on mechanical behaviour of three calcarenite varieties was studied. With this purpose, rock specimens were moistened with different water contents using two different wetting procedures (water immersion and oven drying processes) and then, MRI technique and mechanical tests (UCS, E_{st}, BTS and $I_{s(50)}$) were performed.

It is widely known that a full water saturation of rocks causes reductions in their strength and increases in their deformability. The value of this water-weakening effect is highly dependent on the rock type, reflecting the large variability in texture and lithology [79]. After a thorough review of the published literature on this topic, Wong et al. [57] concluded that sedimentary rocks experience higher reductions than igneous and metamorphic rocks. Specifically, they obtained average UCS reductions of 20% in limestones and 40% in sandstones, and E_{st} drops of<60% in limestones and 20% in sandstones. Argillaceous sedimentary rocks (mudstones, marls, siltstones) typically experience higher decreases in these mechanical parameters (40–90%) [17,57]. In the case of the studied calcarenites, the range of average reductions of UCS, E_{st}, BTS and $I_{s(50)}$ after their full water-saturation were 48–56% in S-1, 54–71% in S-2 and 23–45% in S-3. These decreases of mechanical properties are in line with those reported in limestones by several researchers [80,81].

The different petrophysical properties of the three studied calcarenites can justify the moderate dissimilarities observed with regards to the water-weakening effect [57]. The greater reductions in mechanical properties exhibited by S-2 could be attributed to its high porosity [82], the presence of abundant bioturbation [83] and the larger heterogeneity of its micro-fabric and texture (e.g., an important variability of mineral

Table 4
Equations correlating tensile properties (BTS and $I_{s(50)}$) and water content (w and S_r) in the tested rocks depending on the wetting procedure used.

Wetting procedure	Rock material		
	S-1	S-2	S-3
Immersion process	$I_{S(50)} = 4.13 \cdot e^{-0.139w}$ $R^2 = 0.987$	$I_{S(50)} = 1.25 \cdot e^{-0.240w} + 0.63$ $R^2 = 0.992$	$I_{S(50)} = 1.28 \cdot e^{-0.137w} + 1.52$ $R^2 = 0.998$
	$BTS = 5.23 \cdot e^{-0.224w} + 1.63$ $R^2 = 0.981$	$BTS = 2.28 \cdot e^{-0.468w} + 1.69$ $R^2 = 0.996$	$BTS = 2.31 \cdot e^{-0.943w} + 2.72$ $R^2 = 0.989$
	$I_{S(50)} = 4.13 \cdot e^{-0.0069S_r}$ $R^2 = 0.987$	$I_{S(50)} = 1.26 \cdot e^{-0.0194S_r} + 0.61$ $R^2 = 0.993$	$I_{S(50)} = 1.24 \cdot e^{-0.0139S_r} + 1.55$ $R^2 = 0.998$
	$BTS = 5.22 \cdot e^{-0.0116S_r} + 1.65$ $R^2 = 0.978$	$BTS = 2.30 \cdot e^{-0.0377S_r} + 1.67$ $R^2 = 0.994$	$BTS = 2.30 \cdot e^{-0.0972S_r} + 2.72$ $R^2 = 0.990$
Oven drying process	$I_{S(50)} = 2.32 \cdot e^{-1.257w} + 1.82$ $R^2 = 0.994$	$I_{S(50)} = 1.06 \cdot e^{-0.726w} + 0.75$ $R^2 = 0.996$	$I_{S(50)} = 1.07 \cdot e^{-0.540w} + 1.78$ $R^2 = 0.999$
	$BTS = 3.11 \cdot e^{-0.572w} + 3.48$ $R^2 = 0.975$	$BTS = 2.66 \cdot e^{-0.431w} + 1.77$ $R^2 = 0.982$	$BTS = 2.20 \cdot e^{-0.760w} + 2.78$ $R^2 = 0.995$
	$I_{S(50)} = 2.32 \cdot e^{-0.0640S_r} + 1.82$ $R^2 = 0.994$	$I_{S(50)} = 1.06 \cdot e^{-0.0623S_r} + 0.75$ $R^2 = 0.996$	$I_{S(50)} = 1.07 \cdot e^{-0.0512S_r} + 1.78$ $R^2 = 0.999$
	$BTS = 3.08 \cdot e^{-0.0304S_r} + 3.51$ $R^2 = 0.973$	$BTS = 2.68 \cdot e^{-0.0320S_r} + 1.75$ $R^2 = 0.979$	$BTS = 2.19 \cdot e^{-0.0781S_r} + 2.78$ $R^2 = 0.994$

crystal sizes of the terrigenous constituents and a well-sorted carbonate grains) [48,84], which is reflected in its low P- and S-wave velocities [10]. In contrast, the smaller decrease in mechanical parameters showed by S-3 may be principally attributed to the higher quality of its intergranular cementation and its larger pore throat size, as indicated by its high elastic wave velocities. For its part, S-1 displayed intermediate values of its mechanical properties losses, which can be attributed to a complex combination of counteracting properties: on the one hand, its small pore throat size and the presence of bioturbation and, on the other hand, its low porosity.

Both partial saturation procedures are easy to implement in laboratory and allow to prepare calcarenite samples with intermediate S_r values (25–75%) with an adequate precision and in reasonable periods of time. However, MRI technique corroborates that, as pointed out by Zhou et al. [49], the water distribution inside porous network of these rock materials is completely different depending on the wetting procedure used. On the one hand, partial saturated specimens wetted through the immersion process at atmospheric pressure store water molecules in a localised ring-shaped region close to the rock surface that grows with immersion time, as described by Fu et al. [58]. On the other hand, partial saturated specimens moistened through the oven-drying process at 50 °C storage water molecules in a wider volume of its pore network, even for small water contents. This suggests that future testing standards and procedures developed to assess the influence of moisture on rock properties (such as conductivity, diffusivity, mechanical parameters, etc.) should explicitly indicate which wetting process should be used. This would avoid the potential disruptive effect of water distribution on the measurement of these properties and would ensure the repeatability and comparison of results obtained by different researchers. Furthermore, in the oven-dried rock specimens, the evaporation rate imposed by the used drying temperature could be an additional factor that could affect the water distribution inside their pore network. Thus, future research could focus on assessing this matter.

Concerning the effect of moisture on mechanical behaviour of calcarenites, in general terms, the results showed that severe reductions of UCS, E_{st}, $I_{s(50)}$ and BTS happened when S_r values varied from 0 to 50% and then, these mechanical parameters remained practically constant for greater S_r values ($\geq$75%). Specifically, increments in water content as little as 1.5–2.5% in S-1 and as 2–4% in S-2 and S-3 from the dry condition can cause drops higher than 50% of some of their mechanical parameters, which represents a marked water sensitivity. These findings are in accordance with the results obtained in other types of rocks. For example, in sandstones, Hawkins and McConnell [50] reported that 80–90% of the UCS and E_{st} losses happened for S_r values of 13–53% (w $\leq$ 1%) and Demarco et al. [1] informed that UCS reductions greater 50% occurred when the S_r value was lower than 30%; Erguler and Ulusay [17] observed that drops of UCS, E_{st} and BTS ranging from 90 to 93% occurred for w < 2% in clay-bearing rocks; Cherblanc et al. [44] found that 90% of UCS and BTS reductions were exhibited by limestones when they are equilibrated with a 97% relative humidity atmosphere (w = 0.2–2.5%). The pronounced decrease of mechanical properties found in the tested calcarenites after moisten them with small water contents follows a negative tri-parametric exponential function correlating S_r (or w) and mechanical parameters. Notwithstanding the foregoing, in S-1 and in the specimens of S-2 wetted through the immersion process, a best fit was obtained using a simplified model. In particular, a negative bi-parametric exponential function obtained by fixing zero value for the parameter *c*. This model has also been frequently used by some authors for evaluating the relationship between water content and mechanical properties in shales, clayshales, mudshales and mudstones [15,53], coal [46] or sandstones [45].

Another important outcome derived from this work was that specimens of a given calcarenite with identical water contents but moistened using different saturation processes exhibited dissimilar mechanical properties. Accordingly, the values of the constants of the fitting functions (*a*, *b* and *c*) were also different for each wetting procedure. In particular, for small water contents (S_r = 25 or 50%), the reductions of compressive properties (UCS and E_{st}) were commonly more pronounced in the specimens moistened using the oven-drying process than in those prepared through the immersion process. This could be justified by the fact that water molecules of the specimens prepared through the drying process are mainly concentrated in the central region of the specimens. In contrast, a scarce quantity of water is located in the central zone of the specimens wetted through the immersion process. In this connection, previous testing and numerical simulations of rock materials under uniaxial compression performed using the Finite Element Method (FEM) and the Smooth Particles Hydrodynamics (SPH) technique have suggested that this central zone would be where samples exhibit the most severe damage and deformation [85]. In addition, strength, fracture initiation and propagation and elastic behaviour of rocks are generally governed by pre-existing flaws such as microcracks, voids, pores or grain boundaries [86-88] that could be located randomly inside the specimens. In this sense, due to water is distributed in a greater volume of the pore network in the specimens prepared using the drying process, it is statistically more likely that water molecules are closer to these critical flaws that control the failure, which could also explain the greatest water-weakening effect observed in this case. By contrast, for greater water contents (S_r > 50%), the decreases of these properties were quite similar for both wetting processes, which could be attributed to the fact that water occupies a wider and more alike volume inside the samples.

The influence of the wetting procedure on the two tensile strength parameters ($I_{s(50)}$ and BTS) is considerably different in each of them. On the one hand, partial-saturated samples of the three calcarenite varieties prepared with similar water contents through the drying process exhibited much less $I_{s(50)}$ values than those moistened using the immersion process. This result might be attributed to the abovementioned reason for compressive properties, that is, the greater presence of water molecules in the inner zone of the specimens prepared using the drying process in comparison with those wetted using the immersion process. In this regard, analytical solutions and FEM studies on the stress distribution within a solid circular cylinder subjected to diametral point loads

Fig. 14. Failure patterns obtained in uniaxial compression tests for specimens prepared with different degrees of saturation (S_r) by using the immersion (IP) and drying (DP) procedures. AS: Axial splitting; SF: Shear-dominated failure; CF: Combined failure.

have indicated that the tensile stress at the central part of the specimens determines the fracture load [89-92]. On the other hand, very similar BTS values were found for specimens prepared with the same moisture content despite using different wetting processes. At first sight, this finding may seem a bit striking due to the similarities between Brazilian and diametral Point Load tests with regard to the way in which the load is applied. In this sense, analytical, numerical and experimental previous works have demonstrated that during BTS test the tensile stress is maximum at the centre of the specimen and that crack initiation occurs in the middle of the disc and then propagates to its top and bottom surfaces for the used loading configuration (flat loading platens) [93-96]. However, this result may be related to the higher diameter and the smaller thickness-diameter ratio of the specimens used in the Brazilian test (L/D≈0.5) compared to those used in the diametral Point Load Test (L/D $\geq$ 1). This different shape of the samples results in a different water distribution even though they were prepared with an identical procedure. In other words, water molecules occupy the central region of the specimens during BTS test for both wetting process and for all tested water contents but this does not happen in the PLT specimens. All these observations highlight the key role played by water distribution on the mechanical behaviour of tested calcarenites.

Petrological and physical characteristics of calcarenites and the joint analysis of the effect of water distribution and moisture content on their mechanical behaviour would help to elucidate the main water-weakening mechanisms that affect these rock materials.

The sharp decrease of mechanical properties obtained in the studied calcarenites for low water contents (S_r < 50%) suggests that capillary suction decrease is probably the main mechanism that control the weakening in these materials. Capillarity develops at the interface among materials due to surface tension. More specifically, at small S_r values, water is bounded in the spaces between the grains and pores creating capillary menisci [97]. Surface tension at the border among water and air in contiguous void causes a compressive contact pressure that induces an extra friction resistance [98]. This supplementary

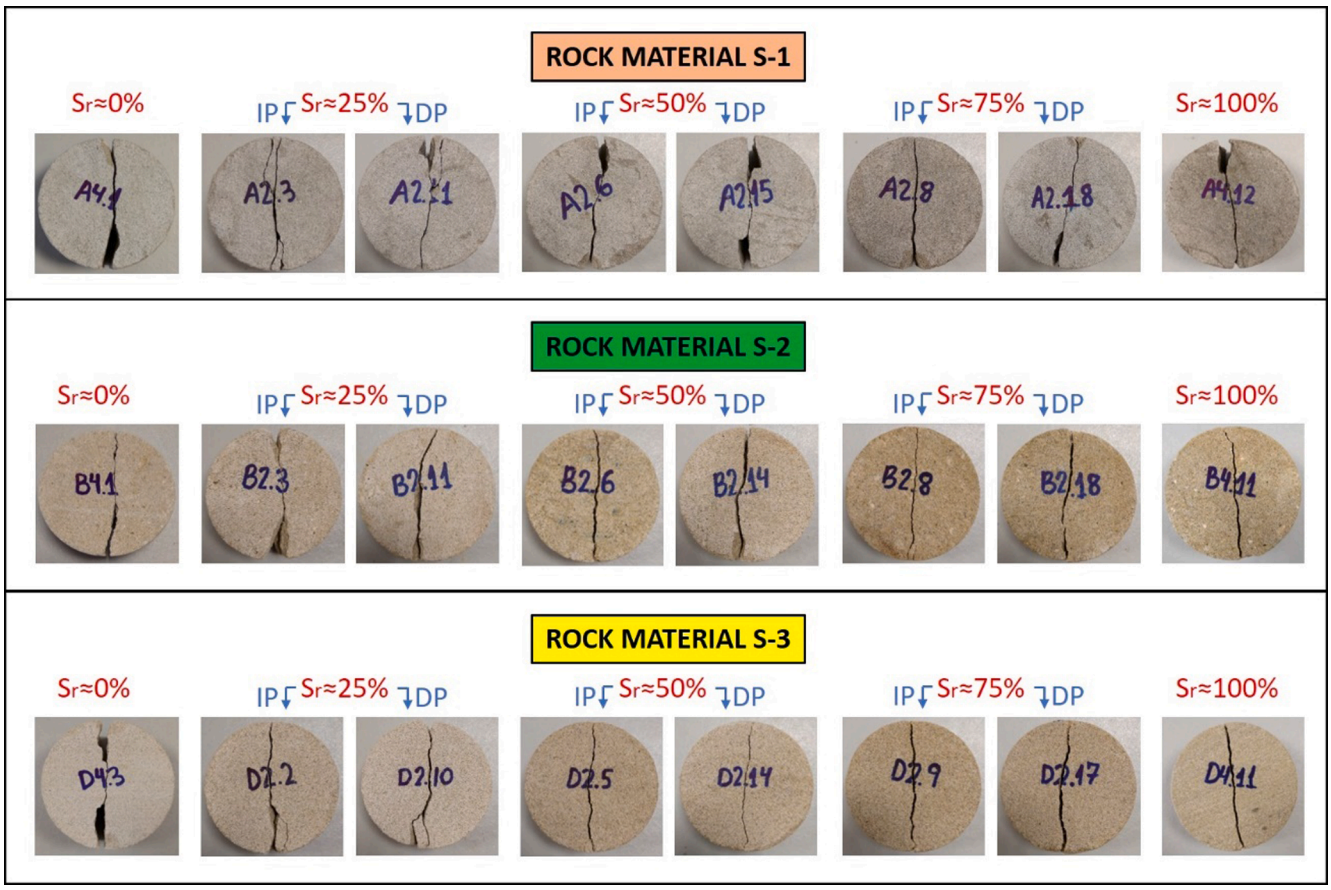

Fig. 15. Failure patterns obtained in Brazilian Tensile Strength tests for specimens prepared with different degrees of saturation (S_r) by using the immersion (IP) and drying (DP) procedures.

resistance has the same effect as if the grains were held together with a cohesive strength component [99]. At higher S_r values, the voids among grains are filled by water, the surface tension intensely diminishes and the corresponding contact pressure disappears [98]. In addition, the different correlations between water content and mechanical parameters obtained by using each wetting procedure reinforces that idea, since capillary action is dissimilar for capillary spaces during immersion and drying processes [49]. Conversely, the fact that important reductions of mechanical parameters occur at water content values associated to small degrees of saturation indicates that pore pressure increase during loading is not a significant cause of the observed weakening. In other words, pore pressure impact would be only relevant when pore network is fully or nearly fully saturated but not when these calcarenites present a scarce water content [50]. In addition, since these calcarenites exhibit high open porosity and permeability, the dissipation of pore pressure must be almost instantaneous and a decrease of the effective stress during load application could hardly have happened [47].

Physicochemical effects such as the dissolution of minerals could probably justify a portion of the observed mechanical weakening. In particular, tested calcarenites exhibit important quantities of calcite grains whose size could be reduced by dissolution [32]. Also, they present small amounts of chlorite and sparite calcite cement that could also be dissolved, leading an increment of rock porosity that could induce their deterioration [79,100]. Nevertheless, the contribution of this phenomenon to the observed debilitation may have been only moderate due to the solubility of calcite in water is a low process (although it could enhance under stresses) [101]. In this connection, it is important to note that these rock materials were exposed to water very short periods of time and the colour of water in the vessel was not substantially altered. Additionally, the swelling of clay minerals (such as illite or smectite) could be responsible of one part of the observed softening. These minerals can induce the breakage of cementation and the formation of microcracks [33,102]. However, this phenomenon would also be of little significance, since the content of these clay minerals is scarce in the three tested calcarenites.

Fracture energy decrease with increasing water content (Rehbinder effect) could be another mechanism that could partially explain the strength reduction found in the studied calcarenites. This theory, that is based on Griffith's fracture criterion, holds that moisture reduces the energy required per unit for the advance of the crack and, therefore, the tensile stress to cause crack growth [37,40]. Also, the considerable presence of quartz in tested calcarenites could play a key role in the detected mechanical weakening. That is, the stresses silicon-oxygen bonds at crack tip may be hydrolysed and debilitated, allowing the cracks to propagate more quickly (stress corrosion) [8,35,36,103,104].

The significant water-weakening effect observed in these calcarenites recalls the need to adequately select the moisture content to use in laboratory to characterise this type of materials, which traditionally have been tested in dry state or with uncontrolled water contents. In this line, some material testing standards [105] and the ISRM Suggested Methods [61] have already drawn attention to this fact and recommended that specimens should be tested with their natural water content. However, this study goes a step further and suggests that, for major engineering projects in which the evaluation of moisture sensitivity is required, the wetting procedure used should be selected carefully, since water distribution plays an important role on mechanical behaviour of rocks. In this connection, since different empirical relationships have been established to estimate the mechanical properties of calcarenites depending on whether are in the process of wetting or drying, the choice of the appropriate equation requires prior clarification of this issue on

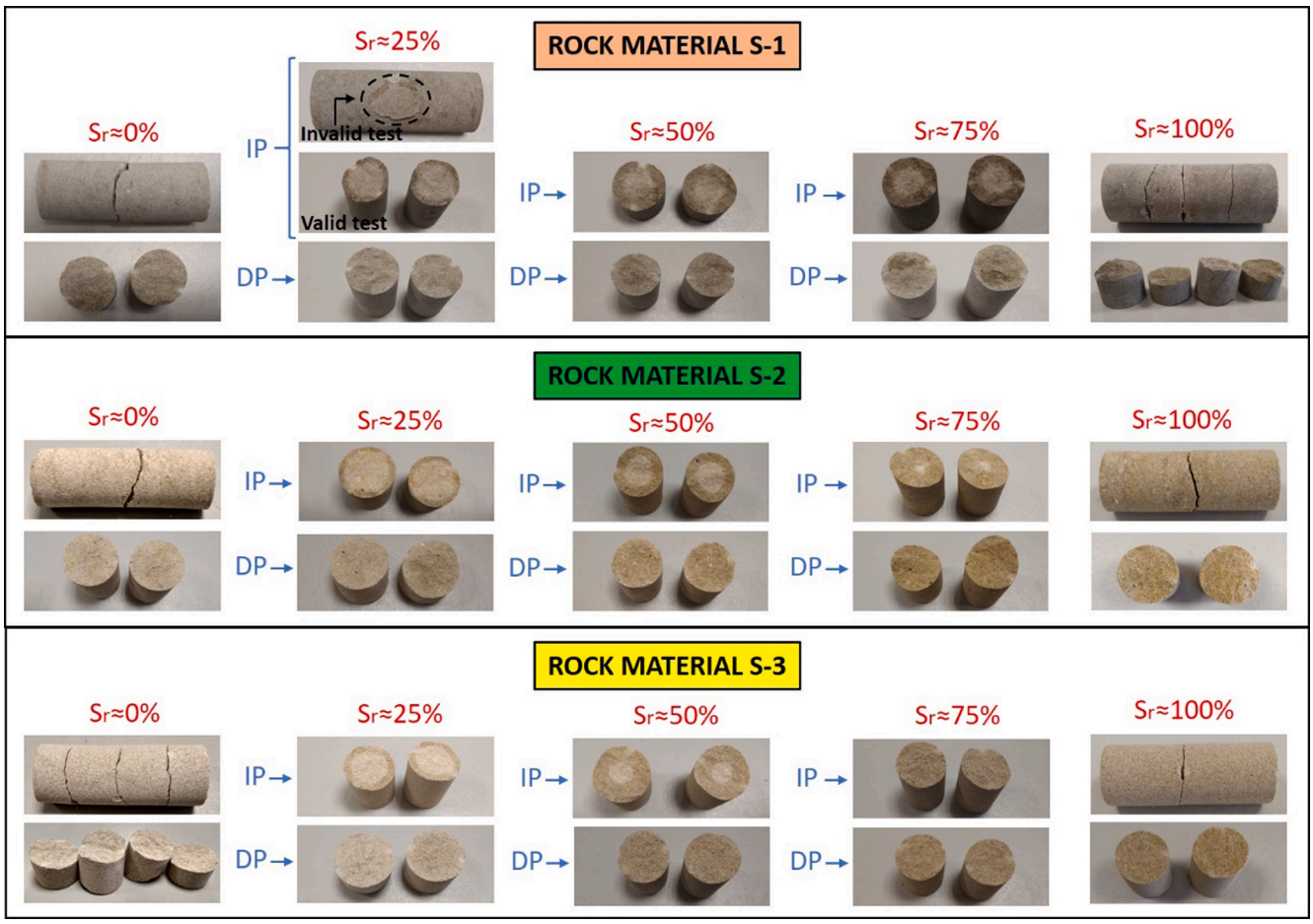

Fig. 16. Failure patterns obtained in Point Load tests for specimens prepared with different degrees of saturation (S_r) by using the immersion (IP) and drying (DP) procedures.

site. In a partially-saturated wall within a building, this matter can be mainly inferred from a carefully analysis of pluviometric, humidity and temperature real-time data in the building environment. Similarly, in a partially-saturated rock mass, continuous information about piezometric level is needed for this purpose. Additionally, for rock masses containing fractures and discontinuities, the presented equations would require upscaling to be relevant since they only provide the matrix strength and do not take meso- or macro-scale fractures into account. With respect to unmonitored and small construction works in which this data is not available, it would be advisable to use directly the equations derived from the drying process with the aim to be on the safety side.

5. Conclusions

Based on the experimental work and the analyses performed in the present paper, the following conclusions can be derived:

(1) MRI technique revealed that during the immersion process water gradually enters from the surface to the core of specimens. By contrast, during the oven-drying process water is progressively removed from the surface to the core. As a consequence, for two samples with the same S_r value, the water distribution inside pore network of partially saturated calcarenites is significantly different in each case. Specifically, specimens wetted through the immersion procedure exhibit a more non-homogeneous water distribution because water molecules are concentrated in a ring-shaped region close to the external surface of the rock. On the contrary, in specimens prepared using the drying procedure, water is distributed more homogenously and occupies a wider volume of sample.

(2) Significant reductions of compression properties (UCS and E_{st}) were obtained when moisture increased in the three calcarenite varieties. Specifically, different negative exponential functions can be used to describe the relationships between these mechanical parameters and water content depending on the lithotype and the wetting procedure used. In this sense, for low water contents ($S_r \leq 50\%$), the decreases of UCS and E_{st} obtained in specimens prepared through the drying process were frequently greater than those observed in specimens wetted through the immersion process. However, for high water contents ($S_r > 50\%$), the reductions were quite similar for both wetting procedures.

(3) Substantial drops of tensile properties (BTS and $I_{s(50)}$) were found when moisture rose in the tested calcarenites. In particular, different negative exponential models were proposed to represent the variation of these properties with water content depending on the rock variety and the wetting procedure used. In this connection, for all partial water saturation conditions (S_r values of 25, 50 and 75%), the reductions of $I_{s(50)}$ found in specimens wetted through the drying process were considerably higher than those obtained in specimens moistened using the immersion process. In the case of BTS, the reductions were very similar for both wetting procedures.

(4) The abovementioned different values of the mechanical properties for the same degrees of saturation obtained in tested calcarenites can be attributed to the conjunction of two factors: (1) the dissimilar water distribution inside the pore network for each wetting procedure and (2) the main water-weakening mechanisms that affects to these rock types (capillary suction decreases and physicochemical effects). In addition, the relationships between all the mechanical properties change slightly depending on the wetting procedure. Therefore, for civil engineering

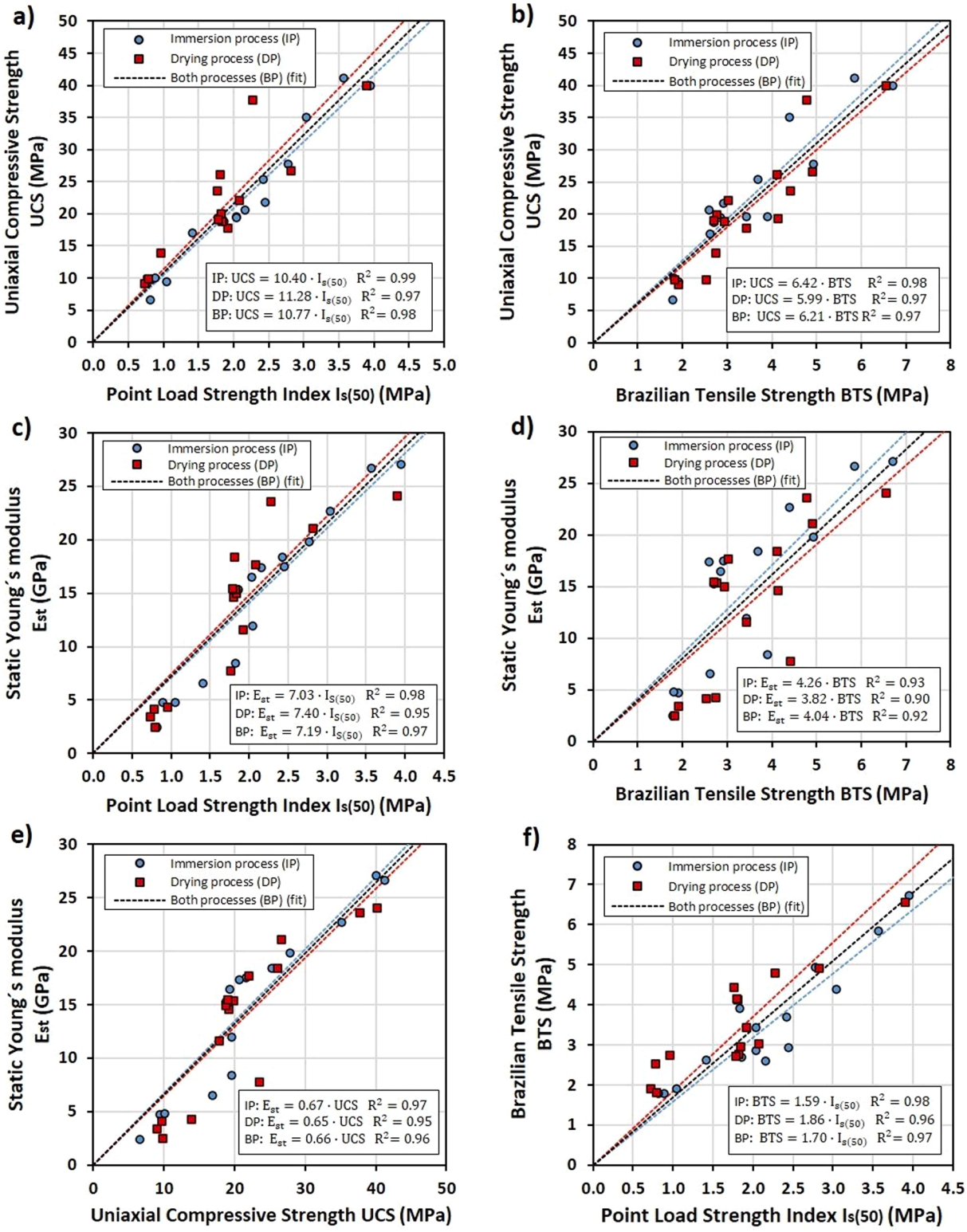

Fig. 17. Correlation functions between the mechanical properties (UCS, E_{st}, BTS and $I_{s(50)}$) for the tested rocks depending on the procedure used to obtain specimens with different water contents.

and architectural works in which the assessment of water sensitivity of mechanical properties of calcarenites is required, the saturation procedure used in laboratory should be cautiously chosen.

CRediT authorship contribution statement

Á. Rabat: Conceptualization, Data curation, Formal analysis, Funding acquisition, Investigation, Methodology, Writing - original draft, Writing - review & editing, Project administration. **R. Tomás:** Conceptualization, Funding acquisition, Resources, Supervision, Validation,

Writing - review & editing. **M. Cano:** Conceptualization, Funding acquisition, Resources, Supervision, Validation, Writing - review & editing.

Declaration of Competing Interest

The authors declare that they have no known competing financial interests or personal relationships that could have appeared to influence the work reported in this paper.

Acknowledgements

This research was supported by the Vice-rector of Research and Knowledge Transfer of the University of Alicante through predoctoral grant FPUUA53-2018 and projects UAUSTI18-21, UAUSTI19-25, UAUSTI20-20, UAEEBB2018-09 and GRE18-15 and by the Spanish Ministry of Economy and Competitiveness (MINECO) through the project TEC2017-85244-C2-1-P. The authors thank to David Castejón and Encarnación Fernández-Valle (Complutense University of Madrid) for providing MR images and photographs of the Fig. 1. They also thank to professor J.C. Cañaveras (University of Alicante) for allowing us to perform the thin-section analyses in his laboratory, to professor David Benavente (University of Alicante) for his advice in the permeability estimation, and to the company "Bateig Piedra Natural S.A" for providing rock material used in this work and the capillarity tests of the studied rocks.

References

[1] M.M. Demarco, E. Jahns, J. Rüdrich, P. Oyhantcabal, S. Siegesmund, The impact of partial water saturation on rock strength: an experimental study on sandstone, Zeitschrift Der Dtsch. Gesellschaft Für Geowissenschaften. 158 (4) (2008) 869–882, https://doi.org/10.1127/1860-1804/2007/0158-0869.

[2] N. Reviron, T. Reuschlé, J.D. Bernard, The brittle deformation regime of water-saturated siliceous sandstones, Geophys. J. Int. 178 (2009) 1766–1778, https://doi.org/10.1111/j.1365-246X.2009.04236.x.

[3] P.L.P. Wasantha, P.G. Ranjith, Water-weakening behavior of Hawkesbury sandstone in brittle regime, Eng. Geol. 178 (2014) 91–101, https://doi.org/10.1016/j.enggeo.2014.05.015.

[4] N.J. Price, The compressive strength of coal measure rocks, Colliery Eng. 37 (1960) 283–292.

[5] R.L. Mann, I. Fatt, Effect of pore fluids on the elastic properties of sandstone, Geophysics. 25 (2) (1960) 433–444, https://doi.org/10.1190/1.1438713.

[6] P.S.B. Colback, B.L. Wiid, The influence of moisture content on the compressive strength of rock, in: Proc. 3rd Can. Rock Mech. Symp., 1965: pp. 65–83.

[7] C.G. Dyke, L. Dobereiner, Evaluating the strength and deformability of sandstones, Q. J. Eng. Geol. Hydrogeol. 24 (1) (1991) 123–134, https://doi.org/10.1144/GSL.QJEG.1991.024.01.13.

[8] J. Hadizadeh, R.D. Law, Water-weakening of sandstone and quartzite deformed at various stress and strain rates, Int. J. Rock Mech. Min. Sci. Geomech. Abstr. 28 (5) (1991) 431–439, https://doi.org/10.1016/0148-9062(91)90081-V.

[9] A. Shakoor, E.H. Barefield, Relationship between unconfined compressive strength and degree of saturation for selected sandstones, Environ. Eng. Geosci. 15 (1) (2009) 29–40, https://doi.org/10.2113/gseegeosci.15.1.29.

[10] E. Verstrynge, R. Adriaens, J. Elsen, K. Van Balen, Multi-scale analysis on the influence of moisture on the mechanical behavior of ferruginous sandstone, Constr. Build. Mater. 54 (2014) 78–90, https://doi.org/10.1016/j.conbuildmat.2013.12.024.

[11] Á. Rabat, M. Cano, R. Tomás, Effect of water saturation on strength and deformability of building calcarenite stones: correlations with their physical properties, Constr. Build. Mater. 232 (2020) 1–15, https://doi.org/10.1016/j.conbuildmat.2019.117259.

[12] M.J. Heap, M. Villeneuve, A.R.L. Kushnir, J.I. Farquharson, P. Baud, T. Reuschlé, Rock mass strength and elastic modulus of the Buntsandstein: an important lithostratigraphic unit for geothermal exploitation in the Upper Rhine Graben, Geothermics. 77 (2019) 236–256, https://doi.org/10.1016/j.geothermics.2018.10.003.

[13] A.R. Jumikis, Some engineering aspects of brunswick shale, 1st ISRM Congr. (1966).

[14] E.M. Van Eeckhout, S.S. Peng, The effect of humidity on the compliances of coal mine shales, Int. J. Rock Mech. Min. Sci. 12 (11) (1975) 335–340, https://doi.org/10.1016/0148-9062(75)90166-7.

[15] G.R. Lashkaripour, R. Ajalloeian, The effect of water content on the mechanical behaviour of fine-grained sedimentary rocks, ISRM Int. Symp. 2000.

[16] Q. Jiang, J. Cui, X. Feng, Y. Jiang, Application of computerized tomographic scanning to the study of water-induced weakening of mudstone, Bull. Eng. Geol. Environ. 73 (4) (2014) 1293–1301, https://doi.org/10.1007/s10064-014-0597-5.

[17] Z.A. Erguler, R. Ulusay, Water-induced variations in mechanical properties of clay-bearing rocks, Int. J. Rock Mech. Min. Sci. 46 (2) (2009) 355–370, https://doi.org/10.1016/j.ijrmms.2008.07.002.

[18] I. Yilmaz, Influence of water content on the strength and deformability of gypsum, Int. J. Rock Mech. Min. Sci. 47 (2) (2010) 342–347, https://doi.org/10.1016/j.ijrmms.2009.09.002.

[19] Á. Rabat, M. Cano, R. Tomás, Á.E. Tamayo, L.R. Alejano, Evaluation of strength and deformability of soft sedimentary rocks in dry and saturated conditions through needle penetration and point load tests: a comparative study, Rock Mech. Rock Eng. 53 (6) (2020) 2707–2726, https://doi.org/10.1007/s00603-020-02067-6.

[20] O. Ojo, N. Brook, The effect of moisture on some mechanical properties of rock, Min. Sci. Technol. 10 (2) (1990) 145–156, https://doi.org/10.1016/0167-9031(90)90158-O.

[21] H. Karakul, R. Ulusay, Empirical correlations for predicting strength properties of rocks from P-wave velocity under different degrees of saturation, Rock Mech. Rock Eng. 46 (5) (2013) 981–999, https://doi.org/10.1007/s00603-012-0353-8.

[22] L.N.Y. Wong, M.C. Jong, Water saturation effects on the brazilian tensile strength of gypsum and assessment of cracking processes using high-speed video, Rock Mech. Rock Eng. 47 (4) (2014) 1103–1115, https://doi.org/10.1007/s00603-013-0436-1.

[23] R. Gholami, V. Rasouli, Mechanical and elastic properties of transversely isotropic slate, Rock Mech. Rock Eng. 47 (5) (2014) 1763–1773, https://doi.org/10.1007/s00603-013-0488-2.

[24] E. Broch, Estimation of strength anisotropy using the point-load test, Int. J. Rock Mech. Min. Sci. 20 (4) (1983) 181–187, https://doi.org/10.1016/0148-9062(83)90942-7.

[25] M. Kohno, H. Maeda, Relationship between point load strength and uniaxial compressive strength of hydrothermally altered soft rocks, Int. J. Rock Mech. Min. Sci. 50 (2012) 147–157, https://doi.org/10.1201/b11646-121.

[26] S. Kahraman, The determination of uniaxial compressive strength from point load strength for pyroclastic rocks, Eng. Geol. 170 (2014) 33–42, https://doi.org/10.1016/j.enggeo.2013.12.009.

[27] D. Li, Z. Sun, Q. Zhu, K. Peng, Triaxial loading and unloading tests on dry and saturated sandstone specimens, Appl. Sci. 9 (2019) 1–19, https://doi.org/10.3390/app9081689.

[28] Á. Rabat, R. Tomás, M. Cano, T. Miranda, Impact of water on peak and residual shear strength parameters and triaxial deformability of high-porosity building calcarenite stones: interconnection with their physical and petrological characteristics, Constr. Build. Mater. 262 (2020) 1–20, https://doi.org/10.1016/j.conbuildmat.2020.120789.

[29] X. Cai, Z. Zhou, H. Zang, Z. Song, Water saturation effects on dynamic behavior and microstructure damage of sandstone: Phenomena and mechanisms, Eng. Geol. 276 (2020) 105760, https://doi.org/10.1016/j.enggeo.2020.105760.

[30] M. Korkanç, Deterioration of different stones used in historical buildings within Nigde province, Cappadocia, Constr. Build. Mater. 48 (2013) 789–803, https://doi.org/10.1016/j.conbuildmat.2013.07.033.

[31] G.H. Newman, Effect of water chemistry on the laboratory compression and permeability characteristics of some north sea chalks, J. Pet. Technol. 35 (1983) 976–980, https://doi.org/10.2118/10203-PA.

[32] M.O. Ciantia, R. Castellanza, C. di Prisco, Experimental study on the water-induced weakening of calcarenites, Rock Mech. Rock Eng. 48 (2) (2015) 441–461, https://doi.org/10.1007/s00603-014-0603-z.

[33] B. Li, J. Liu, K. Bian, F. Ai, X. Hu, M. Chen, Z. Liu, Experimental study on the mechanical properties weakening mechanism of siltstone with different water content, Arab. J. Geosci. 12 (21) (2019), https://doi.org/10.1007/s12517-019-4852-8.

[34] B.K. Atkinson, P.G. Meredith, Stress corrosion cracking of quartz: a note on the influence of chemical environment, Tectonophysics. 77 (1-2) (1981) T1–T11, https://doi.org/10.1016/0040-1951(81)90157-8.

[35] T.A. Michalske, S.W. Freiman, A molecular interpretation of stress corrosion in silica, Nature. 295 (5849) (1982) 511–512, https://doi.org/10.1038/295511a0.

[36] Y. Nara, K. Morimoto, T. Yoneda, N. Hiroyoshi, K. Kaneko, Effects of humidity and temperature on subcritical crack growth in sandstone, Int. J. Solids Struct. 48 (7-8) (2011) 1130–1140, https://doi.org/10.1016/j.ijsolstr.2010.12.019.

[37] P.A. Rehbinder, E.D. Shchukin, Surface phenomena in solids during deformation and fracture processes, Prog. Surf. Sci. 3 (1972) 92–188, https://doi.org/10.1016/0079-6816(72)90011-1.

[38] P. Delage, C. Schroeder, Y.J. Cui, Subsidence and capillary effects in chalks, in: G. Barla (Ed.), ISRM Int. Symp. - EUROCK 96, Balkema, Rotterdam, 1996: pp. 1291–1298.

[39] S. Taibi, A. Duperret, J.-M. Fleureau, The effect of suction on the hydro-mechanical behaviour of chalk rocks, Eng. Geol. 106 (1-2) (2009) 40–50, https://doi.org/10.1016/j.enggeo.2009.02.012.

[40] E.M. Van Eeckhout, The mechanisms of strength reduction due to moisture in coal mine shales, Int. J. Rock Mech. Min. Sci. Geomech. 13 (2) (1976) 61–67, https://doi.org/10.1016/0148-9062(76)90705-1.

[41] P. Baud, W. Zhu, T.-F. Wong, Failure mode and weakening effect of water on sandstone, J. Geophys. Res. Res. 105 (B7) (2000) 16371–16389, https://doi.org/10.1029/2000JB900087.

[42] D. Li, W. Wang, Quantitative analysis of the influence of saturation on rock strength reduction considering the distribution of water, Geomech. Geophys. Geo-Energy Geo-Resources. 5 (2) (2019) 197–207, https://doi.org/10.1007/s40948-019-00106-3.

[43] B. Kleb, B. Vásárhelyi, Test results and empirical formulas of rock mechanical parameters of rhyolitic tuff samples from Eger's cellars, Acta Geol. Hungarica. 46 (3) (2003) 301–312, https://doi.org/10.1556/AGeol.46.2003.3.5.
[44] F. Cherblanc, J. Berthonneau, P. Bromblet, V. Huon, Influence of water content on the mechanical behaviour of limestone: role of the clay minerals content, Rock Mech. Rock. 49 (6) (2016) 2033–2042, https://doi.org/10.1007/s00603-015-0911-y.
[45] H. Masoumi, J. Horne, W. Timms, establishing empirical relationships for the effects of water content on the mechanical behavior of gosford sandstone, Rock Mech. Rock Eng. 50 (8) (2017) 2235–2242, https://doi.org/10.1007/s00603-017-1243-x.
[46] Q. Yao, X. Li, J. Zhou, M. Ju, Z. Chong, B. Zhao, Experimental study of strength characteristics of coal specimens after water intrusion, Arab. J. Geosci. 8 (9) (2015) 6779–6789, https://doi.org/10.1007/s12517-014-1764-5.
[47] M.R. Vergara, T. Triantafyllidis, Influence of water content on the mechanical properties of an argillaceous swelling rock, Rock Mech. Rock Eng. 49 (7) (2016) 2555–2568, https://doi.org/10.1007/s00603-016-0938-8.
[48] Á. Rabat, R. Tomás, M. Cano, Evaluation of mechanical weakening of calcarenite building stones due to environmental relative humidity using the vapour equilibrium technique, Eng. Geol. 278 (2020) 1–20.
[49] Z. Zhou, X. Cai, W. Cao, X. Li, C. Xiong, Influence of water content on mechanical properties of rock in both saturation and drying processes, Rock Mech. Rock Eng. 49 (8) (2016) 3009–3025, https://doi.org/10.1007/s00603-016-0987-z.
[50] A.B. Hawkins, B.J. McConnell, Sensitivity of sandstone strength and deformability to changes in moisture content, Q. J. Eng. Geol. Hydrogeol. 25 (2) (1992) 115–130, https://doi.org/10.1144/GSL.QJEG.1992.025.02.05.
[51] M. Ghafoori, D.W. Airey, J.P. Carter, Correlation of moisture content with the uniaxial compressive strength of ashfield shale, Aust. Geomech. 24 (1993) 112–114.
[52] M. Romana, B. Vásárhelyi, A discussion on the decrease of unconfined compressive strength between saturated and dry rock samples, Proc. 11th Congr. Int. Soc. Rock Mech. 1 (2007) 139–142.
[53] T. AL-Bazali, The impact of water content and ionic diffusion on the uniaxial compressive strength of shale, Egypt. J. Pet. 22 (2013) 249–260, https://doi.org/10.1016/j.ejpe.2013.06.004.
[54] S.R. Wang, P. Hagan, Y.C. Li, C.G. Zhang, X.L. Liu, Experimental study on deformation and strength characteristics of sandstone with different water contents, J. Eng. Sci. Technol. Rev. 10 (4) (2017) 199–203.
[55] S. Tang, The effects of water on the strength of black sandstone in a brittle regime, Eng. Geol. 239 (2018) 167–178, https://doi.org/10.1016/j.enggeo.2018.03.025.
[56] S.B. Tang, C.Y. Yu, M.J. Heap, P.Z. Chen, Y.G. Ren, The influence of water saturation on the short- and long-term mechanical behavior of red sandstone, Rock Mech. Rock Eng. 51 (9) (2018) 2669–2687, https://doi.org/10.1007/s00603-018-1492-3.
[57] L.N.Y. Wong, V. Maruvanchery, G. Liu, Water effects on rock strength and stiffness degradation, Acta Geotech. 11, 2016, 713–737, https://doi.org/10.1007/s11440-015-0407-7.
[58] T.-F. Fu, T. Xu, M.J. Heap, P.G. Meredith, T.-H. Yang, T.M. Mitchell, Y. Nara, Analysis of capillary water imbibition in sandstone via a combination of nuclear magnetic resonance imaging and numerical DEM modeling, Eng. Geol. 285 (2021) 106070, https://doi.org/10.1016/j.enggeo.2021.106070.
[59] H. Liu, W. Zhu, Y. Yu, T. Xu, R. Li, X. Liu, Effect of water imbibition on uniaxial compression strength of sandstone, Int. J. Rock Mech. Min. Sci. 127 (2020) 104200, https://doi.org/10.1016/j.ijrmms.2019.104200.
[60] C. Franzen, P.W. Mirwald, Moisture content of natural stone: Static and dynamic equilibrium with atmospheric humidity, Environ. Geol. 46 (2004) 391–401, https://doi.org/10.1007/s00254-004-1040-1.
[61] ISRM, The Complete ISRM Suggested Methods for Rock Characterization, Testing and Monitoring: 1974–2006, Comm. Test. Methods, Int. Soc. Rock Mech. ISRM Turkish Natl. Group, Ankara. 3, 2007.
[62] AENOR, UNE-EN 1936. Métodos de ensayo para piedra natural. Determinación de la densidad real y aparente y de la porosidad abierta y total., Asoc. Española Norm. y Certificación, Madrid, 2007.
[63] AENOR, UNE 103-302-94. Determinación de la densidad relativa de las partículas de un suelo., Asoc. Española Norm. y Certificación, Madrid. (1994) 4.
[64] A. Paar, Quantachrome Instruments, Quantachrome Instruments. (2018). http://www.quantachrome.com/ (accessed July 7, 2021).
[65] Bateig, Piedra Natural-Bateig, Características. (2021). https://bateig.com/ (accessed July 13, 2021).
[66] D. Benavente, C. Pla, N. Cueto, S. Galvañ, J. Martínez-Martínez, M.A. García-del-Cura, S. Ordóñez, Predicting water permeability in sedimentary rocks from capillary imbibition and pore structure, Eng. Geol. 195 (2015) 301–311, https://doi.org/10.1016/j.enggeo.2015.06.003.
[67] AENOR, UNE-EN 14579. Método de ensayo para piedra natural. Determinación de la velocidad de propagación del sonido., Asoc. Española Norm. y Certificación, Madrid, 2005.
[68] V.P.B. Grover, J.M. Tognarelli, M.M.E. Crossey, I.J. Cox, S.D. Taylor-Robinson, M. J.W. McPhail, Magnetic resonance imaging: principles and techniques: lessons for clinicians, J. Clin. Exp. Hepatol. 5 (3) (2015) 246–255, https://doi.org/10.1016/j.jceh.2015.08.001.
[69] ISRM, Suggested, Methods for determining the uniaxial compressive strength and deformability of rock materials, Int. Soc. Rock Mech. (1977).
[70] A. Nicolas, J. Fortin, J.B. Regnet, B.A. Verberne, O. Plümper, A. Dimanov, C. J. Spiers, Y. Guéguen, Brittle and semibrittle creep of Tavel limestone deformed at room temperature, J. Geophys. Res. Solid Earth. 122 (6) (2017) 4436–4459, https://doi.org/10.1002/jgrb.v122.610.1002/2016JB013557.
[71] N. Brantut, M.J. Heap, P. Baud, P.G. Meredith, Mechanisms of time-dependent deformation in porous limestone, J. Geophys. Res. Solid Earth. 119 (7) (2014) 5444–5463, https://doi.org/10.1002/2014JB011186.
[72] J.A. Franklin, Suggested method for determining point load strength, Int. J. Rock Mech. Min. Sci. Geomech. Abstr. 22 (2) (1985) 51–60, https://doi.org/10.1016/0148-9062(85)92327-7.
[73] ASTM, D3967–08: standard test method for splitting tensile strength of intact rock core specimens, ASTM Int. West Conshohocken. (2008), https://doi.org/10.1520/D3967-08.2.
[74] S. Ordoñez, M. Louis, M.A. García del Cura, R. Fort, M.C. López de Azcona, F. Mingarro, Physical properties and petrographic characteristics of some Bateig stone varieties, in: R. Oliveira, A.G. Rodrigues, A.G. Coelho, A.P. Cunha (Eds.), 7th Int, IAEG Congr, Lisboa, 1994, pp. 3595–3603.
[75] R. Fort, A. Bernabeu, M.A. García del Cura, M.C. López de Azcona, S. Ordóñez, F. Mingarro, La Piedra de Novelda: una roca muy utilizada en el patrimonio arquitectónico, Mater. Construcción. 52 (266) (2002) 19–32, https://doi.org/10.3989/mc.2002.v52.i26610.3989/mc.2002.v52.i266.332.
[76] B. Vásárhelyi, P. Ván, Influence of water content on the strength of rock, Eng. Geol. 84 (1-2) (2006) 70–74, https://doi.org/10.1016/j.enggeo.2005.11.011.
[77] R. Nazir, E. Momeni, D.J. Armaghani, M.F.M. Amin, Correlation between unconfined compressive strength and indirect tensile strength of limestone rock samples, Electron. J. Geotech. Eng. 18 I, 2013, 1737–1746.
[78] Z. Li, G. Xu, X. Zhao, Y. Fu, C. Su, Applicability of needle penetration test on soft rocks, Electron. J. Geotech. Eng. 21 (2016) 7209–7222.
[79] X. Cai, Z. Zhou, K. Liu, X. Du, H. Zang, Water-weakening effects on the mechanical behavior of different rock types: phenomena and mechanisms, Appl. Sci. 9 (2019) 14–28, https://doi.org/10.3390/app9204450.
[80] B. Vsrhelyi, Statistical analysis of the influence of water content on the strength of the miocene limestone, Rock Mech. Rock Eng. 38 (1) (2005) 69–76, https://doi.org/10.1007/s00603-004-0034-3.
[81] M.A. Rajabzadeh, Z. Moosavinasab, G. Rakhshandehroo, Effects of rock classes and porosity on the relation between uniaxial compressive strength and some rock properties for carbonate rocks, Rock Mech. Rock Eng. 45 (1) (2012) 113–122, https://doi.org/10.1007/s00603-011-0169-y.
[82] F.G. Bell, The physical and mechanical properties of the fell sandstones, Northumberland, England, Eng. Geol. 12 (1978) 1–29, https://doi.org/10.1016/0013-7952(78)90002-9.
[83] L. Anania, A. Badalà, G. Barone, C.M. Belfiore, C. Calabrò, M.F. La Russa, P. Mazzoleni, A. Pezzino, The stones in monumental masonry buildings of the "val di Noto" area: new data on the relationships between petrographic characters and physical-mechanical properties, Constr. Build. Mater. 33 (2012) 122–132, https://doi.org/10.1016/j.conbuildmat.2011.12.076.
[84] Z. Pápay, Á. Török, Effect of thermal and freeze-thaw stress on the mechanical properties of porous limestone, Period. Polytech. Civ. Eng. 62 (2018) 423–428, https://doi.org/10.3311/PPci.11100.
[85] A. Mardalizad, R. Scazzosi, A. Manes, M. Giglio, Testing and numerical simulation of a medium strength rock material under unconfined compression loading, J. Rock Mech. Geotech. Eng. 10 (2) (2018) 197–211, https://doi.org/10.1016/j.jrmge.2017.11.009.
[86] G.K. Zhang, H.B. Li, M.Y. Wang, X.F. Li, Crack initiation of granite under uniaxial compression tests: a comparison study, J. Rock Mech. Geotech. Eng. 12 (3) (2020) 656–666, https://doi.org/10.1016/j.jrmge.2019.07.014.
[87] M Cai, P.K Kaiser, Y Tasaka, T Maejima, H Morioka, M Minami, Generalized crack initiation and crack damage stress thresholds of brittle rock masses near underground excavations, Int. J. Rock Mech. Min. Sci. 41 (5) (2004) 833–847, https://doi.org/10.1016/j.ijrmms.2004.02.001.
[88] E. Hoek, C.D. Martin, Fracture initiation and propagation in intact rock - a review, J. Rock Mech. Geotech. Eng. 6 (4) (2014) 287–300, https://doi.org/10.1016/j.jrmge.2014.06.001.
[89] K.T. Chau, Analytic solutions for diametral point load strength tests, J. Eng. Mech. 124 (8) (1998) 875–883, https://doi.org/10.1061/(ASCE)0733-9399(1998)124:8(875).
[90] M.S. Al-Derbi, M.H. de Freitas, Use of the boussinesq equation for determining the distribution of stress within a diametrical point load test, Rock Mech. Rock Eng. 32 (4) (1999) 257–265, https://doi.org/10.1007/s006030050047.
[91] G. Wijk, Point load test for the tensile strength of rock, Geotech. Test. J. 3 (1980) 49–54, https://doi.org/10.1520/GTJ10902J.
[92] A. Zacoeb, K. Ishibashi, Point load test application for estimating compressive strength of concrete structures from small core, J. Eng. Appl. Sci. 4 (2009) 46–57.
[93] D. Li, B. Li, Z. Han, Q. Zhu, Evaluation on rock tensile failure of the Brazilian discs under different loading configurations by digital image correlation, Appl. Sci. 10 (2020) 1–17, https://doi.org/10.3390/app10165513.
[94] E. Komurlu, A. Kesimal, S. Demir, Experimental and numerical study on determination of indirect (splitting) tensile strength of rocks under various load apparatus, Can. Geotech. J. 53 (2) (2016) 360–372, https://doi.org/10.1139/cgj-2014-0356.
[95] W.C. Zhu, C.A. Tang, Numerical simulation of Brazilian disk rock failure under static and dynamic loading, Int. J. Rock Mech. Min. Sci. 43 (2) (2006) 236–252, https://doi.org/10.1016/j.ijrmms.2005.06.008.
[96] B.V.D. Steen, A. Vervoort, J.A.L. Napier, Observed and simulated fracture pattern in diametrically loaded discs of rock material, Int. J. Fract. 131 (1) (2005) 35–52, https://doi.org/10.1007/s10704-004-3177-z.
[97] G. West, Effect of suction on the strength of rock, Q. J. Eng. Geol. 27 (1) (1994) 51–56, https://doi.org/10.1144/GSL.QJEGH.1994.027.P1.07.
[98] E. Papamichos, M. Brignoli, F.J. Santarelli, Experimental and theoretical study of a partially saturated collapsible rock, Mech. Cohesive-Frictional Mater. 2 (1997)

251–278, https://doi.org/10.1002/(SICI)1099-1484(199707)2:3<251::AID-CFM33>3.0.CO;2-%23.
[99] K.M. Wild, L.P. Wymann, S. Zimmer, R. Thoeny, F. Amann, Water retention characteristics and state-dependent mechanical and petro-physical properties of a clay shale, Rock Mech. Rock Eng. 48 (2) (2015) 427–439, https://doi.org/10.1007/s00603-014-0565-1.
[100] M.L. Lin, F.S. Jeng, L.S. Tsai, T.H. Huang, Wetting weakening of tertiary sandstones—microscopic mechanism, Environ. Geol. 48 (2) (2005) 265–275, https://doi.org/10.1007/s00254-005-1318-y.
[101] R. Risnes, M.V. Madland, M. Hole, N.K. Kwabiah, Water weakening of chalk - mechanical effects of water-glycol mixtures, J. Pet. Sci. Eng. 48 (1-2) (2005) 21–36, https://doi.org/10.1016/j.petrol.2005.04.004.
[102] M. Tiennot, J.-D. Mertz, A. Bourgès, Influence of clay minerals nature on the hydromechanical and fracture behaviour of stones, Rock Mech. Rock Eng. 52 (6) (2019) 1599–1611, https://doi.org/10.1007/s00603-018-1672-1.
[103] B.K. Atkinson, A fracture mechanics study of subcritical tensile cracking of quartz in wet environments, Pure Appl. Geophys. 117 (5) (1979) 1011–1024, https://doi.org/10.1007/BF00876082.
[104] N. Brantut, M.J. Heap, P.G. Meredith, P. Baud, Time-dependent cracking and brittle creep in crustal rocks: a review, J. Struct. Geol. 52 (2013) 17–43, https://doi.org/10.1016/j.jsg.2013.03.007.
[105] AENOR, UNE 22-950-90-1. Propiedades mecánicas de las rocas. Ensayos para la determinación de la resistencia. Parte 1: Resistencia a la compresión uniaxial., Asoc. Española Norm. y Certificación, Madrid, 1990, 1–4.